Predicting the reactivity of trawl-disturbed sediment carbon from measurable seabed properties

Shahram Asgari[1]

[1]Department of Marine Sciences, University of Georgia, Athens, GA 30602, USA

Correspondence: Shahram Asgari (shahram.asgari@uga.edu)

ORCID: 0009-0004-3810-2739

This is a non-peer-reviewed preprint submitted to EarthArXiv. It has not undergone peer review. The manuscript is intended for submission to the peer-reviewed journal *Biogeosciences*.

Abstract

Mobile bottom-contact fishing gear disturbs a large area of the continental shelf each year. How much carbon that releases depends on how fast the disturbed material is mineralised. Assessments represent that with a first-order rate constant, and because its value is unmeasured they sample it across five orders of magnitude, which makes it their dominant uncertainty. Here the constant is derived instead of assumed. Organic matter arriving at the seabed is described as a reactivity continuum, each component is transported through an accreting and bioturbated bed, and the mass-weighted rate constant of the layer a gear removes follows in closed form. Two independent numerical solutions confirm it. Sweeping the parameters over shelf ranges then shows where the answer comes from. With the arriving material held fixed the rate constant varies 39-fold; letting it vary widens the spread to four orders of magnitude. Four fifths of that wider spread is carried by the age of the arriving material and one thousandth by the depth the gear cuts to. No gear reaches fresh-deposit reactivity at any cutting depth, because reactive components are consumed before they can accumulate: the sediment surface is already 1.4 to 56 times less reactive than the material landing on it. Rapidly accumulating, weakly mixed beds give rate constants about thirty times higher than slowly accumulating, well-mixed beds. Measurement effort should therefore go to the material settling from the water column rather than to the disturbance, but only pays once that material is constrained to within a factor of eight, which no published regional inversion achieves.

Keywords: bottom trawling; organic carbon reactivity; reactive continuum; bioturbation; early diagenesis; continental shelf sediments

Highlights

- Trawling carbon budgets assume the rate at which disturbed sediment carbon breaks down. Here it is derived in closed form from the reactivity mixture arriving at the seabed and three mappable site properties: cutting depth, accumulation rate and mixing intensity.

- Across the conditions found on continental shelves the rate constant spans 1.59 decades, with a median of 5.5×10^{-3} yr^{-1}, when the arriving mixture is known. It spans 4.11 decades when the arriving mixture is unknown.

- Of that wider spread the apparent initial age of the arriving material accounts for 0.792 ± 0.001, and the cutting depth for 0.001. The reactivity of disturbed carbon is set by what settles on the seabed, not by the fishing that disturbs it.

- No gear reaches freshly deposited reactivity, however shallow the cut, because reactive components are consumed before they accumulate. The surface is 1.4 to 56 times less reactive than the arriving material at a fixed mixture, and 1.0 to 131 times once the mixture varies. The shortfall is governed by D_b/w^2 at a fixed mixture and by $D_b/(a\, w^2)$ in general. Estimates built on a fresh-deposit constant are therefore high, by about an order of magnitude in muddy, well-mixed beds.

- Mapping accumulation, mixing and cutting depth removes 1.34 of the 4.11 decades with existing methods. Constraining the arriving material removes more only once its apparent initial age is known to better than 0.91 decades, against the two decades reached so far.

- The ordering survives seven sensitivity analyses: compaction, seasonal supply, depth-dependent mixing, a non-local conveyor, a lognormal continuum and a widened parameter box. The deposited code reproduces every number and figure from the parameter values alone.

1 Introduction

Organic matter arriving at the seabed is a mixture whose components decay at rates spanning many orders of magnitude (Middelburg, 1989; Boudreau and Ruddick, 1991; Arndt et al., 2013). The fast components are consumed first, so the residual grows less reactive as it ages. Reactivity at a given depth is therefore a record of how long that material has been in the bed. Two transport processes set that residence time. Burial carries material downward at the accumulation rate, and burrowing animals mix it through the top few centimetres (Middelburg et al., 1997; Solan et al., 2019). Mixing acts in both directions, returning old material to the surface as well as carrying fresh material down, so sediment age depends jointly on burial velocity and mixing intensity rather than on either alone (Meile and Van Cappellen, 2005). Global compilations use that dependence to fit continuum parameters to measured profiles, and report values that differ systematically between depositional settings (Freitas et al., 2021; Pika et al., 2023; Xu et al., 2023). Mobile bottom-contact fishing gear disturbs a large area of the continental shelf each year, and the carbon this releases is contested. Published estimates span 17 to 400 Mt C yr^{-1}, a range assembled by Khedri et al. (2025); the global figures in it are from Sala et al. (2021) and Atwood et al. (2024), while Epstein et al. (2022) and Hiddink et al. (2023) contest those rather than replace them.

What separates the estimates is not the mass of sediment mobilised, which follows from gear characteristics and vessel monitoring data. It is what becomes of the organic carbon once mobilised, and every assessment represents that by prescribed first-order rate constants. Sala et al. (2021) took values typical of freshly deposited surface material, 0.275 to 16.8 yr^{-1} by region, applied to a labile fraction assigned by sediment type. Hiddink et al. (2023) replied that the bulk sediment a trawl disturbs is far less reactive. Khedri et al. (2025) declined to choose and treated the constant as unknown, sampling its full published range of 10^{-4} to 10^{1} yr^{-1} and propagating the ensemble to 270 kt C yr^{-1} for the northwest European shelf, with an interquartile range of 620 kt C yr^{-1}. They identify reactivity as the leading source of that uncertainty and call for experiments to constrain it.

The forward problem is solved. Kuderer and Middelburg (2024) coupled particle tracking to age-dependent kinetics and showed that bioturbation flattens reactivity profiles, and Rooze et al. (2023) built an Eulerian moment model for age and reactivity continua under mixing. Neither answers the question a trawling assessment asks, which is what rate constant to assign to the particular depth interval a gear removes. Measurement has approached from the other side: Bartl and Thrush (2025) related resuspension-induced CO_2 production at 57 sites to sediment properties, but what they report is an areal flux, not a rate constant. Three ingredients needed to answer that question already exist and have not been composed. Gear penetration depth fixes the depth interval. Accumulation and bioturbation fix how long the material in it has been buried. A reactivity continuum converts that residence time into a rate constant.

This work carries out that composition and then tests what the result depends on. The organic matter reaching the seabed is described as a distribution over first-order rate constants, and for every component in it the steady balance between biodiffusive mixing, burial and decay is solved. The balance is linear, and its coefficients are constant over the few centimetres a gear reaches, so each component has an exponential profile and the rate constant of the disturbed layer reduces to one integral over components. No parameter is fitted: every input is a quantity shelf surveys already report. The result is verified twice, component by component against a collocation solve and, once assembled, against a finite-volume solver that reproduces the quadrature, the surface flux and the depth integration independently. It is then mapped across shelf ranges, its spread is split among the five parameters, and seven assumptions are tested, among them depth-dependent mixing, compaction, a non-local mixing operator, a lognormal continuum and a seasonally varying supply.

2 Methods

2.1 Reactivity continuum of the deposited organic matter

Organic carbon reaching the seabed is a mixture of compounds whose decay rates differ by many orders of magnitude. Instead of tracking individual compounds, the mixture is described by a distribution over first-order decay rate constants. The gamma form of Boudreau and Ruddick (1991) was used, in which the deposited mass density $g(k)$ (yr) depends on the rate constant k (yr^{-1}), a dimensionless shape parameter ν, and the apparent initial age of the mixture a (yr):

$$g(k) = \frac{a^{\nu}\, k^{\nu-1}\, e^{-ak}}{\Gamma(\nu)}. \qquad (1)$$

The shape ν sets how wide the mixture is, and the age a sets where it sits: raising a slides the whole distribution toward lower reactivity without changing its width. The age is apparent rather than real, being the age a mixture of this shape would need in order to be as unreactive as the material observed. Their ratio ν/a is the mean rate constant of the mixture and is used throughout as a single summary of how reactive the arriving material is. Γ(ν) is the gamma function, the standard extension of the factorial to non-integer arguments. It appears here only as the constant that makes $g(k)$ integrate to one, so that the mixture carries unit mass; it has no units, no physical role, and cancels from every result below.

Both parameters are obtained by inversion against field data, although not always together: Freitas et al. (2021) fit ν and a to measured sediment profiles, Pika et al. (2023) hold ν at 0.151 and fit a alone to diffusive oxygen uptake, and Xu et al. (2023) fit a lognormal form instead. The ranges adopted here are listed in Table 2.

A component is defined as all the organic matter that decays at a given rate k. Compounds are grouped by decay rate and by no other property, because no other property enters the calculation. The quadrature of Sect. 2.4 resolves the mixture into 20 000 components. All symbols and units are collected in Table 1.

2.2 Transport and reaction in the bed

Each component is buried, mixed by bioturbation and lost by decay, and exchanges with no other component. Bioturbation is represented as a diffusive flux, which is standard for beds mixed by many small displacements (Boudreau, 1986a; Meysman et al., 2003, 2010). The steady-state mass balance for one component relates its concentration C_k (g C cm^{-3}) to depth below the sediment-water interface z (cm), the biodiffusion coefficient D_b (cm^2 yr^{-1}) and the accumulation rate w (cm yr^{-1}):

$$D_b\, \frac{\mathrm{d}^2 C_k}{\mathrm{d}z^2} - w\, \frac{\mathrm{d}C_k}{\mathrm{d}z} - k\, C_k = 0. \qquad (2)$$

The processes retained in Eq. (2) and those omitted are listed in Table 3.

The biodiffusive closure is a local approximation. It holds when particle displacements are small and frequent relative to the depth interval of interest, so that the flux at any depth is set by the local concentration gradient (Boudreau, 1986a; Meysman et al., 2003). Head-down deposit feeders violate both conditions: ingestion at depth and egestion at the interface displaces particles across the whole feeding zone in a single event, so the flux at a given depth depends on the concentration several centimetres away (Meysman et al., 2010). A non-local operator of that form is substituted for biodiffusion in Sect. 3.2.3, and the resulting shift in k_{dist} is given in Table 5.

D_b is taken as constant over the few centimetres a gear reaches. Equation (2) then has constant coefficients, and every component has an exponential profile. The solution that decays with depth is

$$C_k(z) = C_k(0)\, e^{\lambda_k z}, \qquad \lambda_k = \frac{w - \sqrt{w^2 + 4D_b k}}{2D_b}, \qquad (3)$$

where λ_k (cm^{-1}) is the negative root of $D_b\lambda^2 - w\lambda - k = 0$. The surface concentration follows from the flux condition at the interface: the flux of a component is advective plus diffusive, and at $z = 0$ it equals the depositional supply $F\, g(k)$, so

$$C_k(0) = \frac{F\, g(k)}{w - D_b \lambda_k}, \qquad (4)$$

where F (g C cm^{-2} yr^{-1}) is the total depositional flux of organic carbon. It multiplies every component equally and cancels from Eq. (5), so no result below depends on it.

2.3 The rate constant of the disturbed layer

A gear penetrating to depth PD (cm) removes or resuspends everything above that depth. A one-pool trawling model assigns that material a single rate constant, and the consistent choice is the mass-weighted mean over the components present, k_{dist} (yr^{-1}):

$$k_{\mathrm{dist}}(PD) = \frac{\int_0^\infty \int_0^{PD} k\ C_k(z)\, \mathrm{d}z\, \mathrm{d}k}{\int_0^\infty \int_0^{PD} C_k\,(z)\, \mathrm{d}z\, \mathrm{d}k}. \qquad (5)$$

Each component decays exponentially with depth, so the inner integral has a closed form:

$$\int_0^{PD} C_k\,(z)\, \mathrm{d}z = C_k(0)\, \frac{e^{\lambda_k PD} - 1}{\lambda_k}. \qquad (6)$$

Substituting Eqs. (4) and (6) into Eq. (5) leaves one quadrature over k. Equations (1) to (6) are the whole model. It has five parameters: ν and a describe the arriving mixture, and w, D_b and PD describe the bed and the gear.

2.4 Numerical implementation

The quadrature. The integral over k was evaluated on a logarithmic grid whose limits, resolution and convergence are given in Table 4. The coarsest grid used anywhere costs 5×10^{-5} decades in k_{dist}, three orders of magnitude below the smallest effect any conclusion rests on.

The inert component. For $\nu < 1$ the density in Eq. (1) diverges as $k \to 0$, so any finite lower limit k_{min} omits real mass. That mass reacts too slowly to contribute to the numerator of Eq. (5), but it is not negligible in the denominator. It was therefore carried as an explicit $k = 0$ component of weight $P(\nu, a\, k_{\mathrm{min}})$, the regularised lower incomplete gamma, rather than redistributed by renormalising the grid. Appendix A6 gives its profile and the error renormalisation would introduce. With it carried, the mean rate constant of the deposit is ν/a exactly.

The solver. The scenarios of Sect. 3.2.3 that relax constant D_b, add compaction, or substitute a non-local operator have no closed form and were solved by finite volumes. The upper boundary prescribes the depositional solid flux, the lower applies a radiation condition $\mathrm{d}C_k/\mathrm{d}z = \lambda_k C_k$. A fixed concentration is inadmissible there, because a nearly inert component has an advective decay length w/k longer than any practical domain; Sect. 3.2.3 reports what that substitution costs. Organic carbon is a solid-phase species, so every term carries the solid volume fraction $1 - \varphi$ rather than the porosity φ. Domain length, node count and convergence are in Table 4.

2.4.1 Application

Every range below is a working prior for a northwest European shelf bed. None is fitted, and none is the full span of what has been measured. Where a prior is narrower than the published measurements, that is stated and its effect is tested in Sect. 3.2.3.

Accumulation rate, 0.02 to 0.6 cm yr^{-1}, the interval commonly quoted for shelf muds and sands (Middelburg et al., 1997; Solan et al., 2019).

Biodiffusion, 1 to 150 $cm^2\ yr^{-1}$. This holds about 85 % of the shelf records in the compilation of Solan et al. (2019), whose full spread below 200 m of water runs from 10^{-4} to 6.7×10^3 $cm^2\ yr^{-1}$. It is an envelope for a typical bed, not an outer bound. Kuderer and Middelburg (2024) cite the same sources for 0.001 to 10 $cm^2\ yr^{-1}$, which overlaps the interval used here over exactly one decade, and apply it to coastal, slope and deep-sea settings alike.

Gear penetration depth, 1 to 5 cm, covering the central values assigned to otter trawls, beam trawls and dredges by sediment type (Pitcher et al., 2022; Khedri et al., 2025). Those assignments themselves run from 0 cm on gravel to 5.4 cm for a dredge in mud.

Continuum shape, 0.10 to 0.30, bracketing the 0.1 to 0.2 that Freitas et al. (2021) find in almost all of their inversions and admitting their higher outliers.

Apparent initial age, 1 to 1000 yr. This is the one prior markedly narrower than the measurements. Freitas et al. (2021) report a over 10^{-3} to 10^7 yr, most values falling between 1 and 10^4 yr, and Pika et al. (2023) return 0.6 to 2×10^6 yr. Sect. 3.2.3 therefore repeats the whole decomposition over 0.1 to 10^5 yr.

All five are listed with their sources in Table 2.

The comparison in Sect. 3.3 centres its constraint on an apparent initial age of 10 yr, a plausible shelf value rather than the geometric centre of the prior range, which is 32 yr. Section 3.3 reports what that choice costs.

Seven assumptions were tested rather than asserted. Table 5 gives, for each scenario, what was changed, what it was changed to, and the resulting shift in k_{dist}. Three of the seven were run at two settings each, so the table has more rows than assumptions, and the seventh, the numerical solution itself, is a verification rather than a scenario and appears at the head of Sect. 3.2.3. The parameters that enter only these scenarios are given in Table 5 and used nowhere else: the porosity profile, the mixed-layer taper, the conveyor feeding zone and exchange rate, and the amplitude and period of the deposition cycle.

2.5 Verification and splitting the spread

The solution was verified twice, at two different levels. Equation (3) was checked component by component against an independent collocation solve of Eq. (2), written without shared code, with the depositional flux imposed at the interface and the concentration vanishing at depth. That check cannot reach the quadrature or the inert fraction, so the assembled constant of Eq. (5) was checked separately against the finite-volume solver of Sect. 2.4, which reproduces both independently of the closed form.

The spread was then split among the parameters using Sobol indices, estimated by Saltelli sampling on $\log_{10} k_{\mathrm{dist}}$. A total Sobol index is the share of the variance that one parameter accounts for, including everything it contributes through interactions with the others; it runs from zero, meaning no influence, to one, meaning the parameter alone determines the answer.

Three choices are worth stating. The logarithm was used because the quantity spans decades and because the assessments that consume it sample it log-uniformly. A scrambled Sobol′ lowdiscrepancy sequence replaced pseudo-random draws, because with the latter the first-order index of the dominant parameter exceeded its own total index, which is impossible and signals estimator noise. Uncertainty on each index was taken across five independent scrambles rather than across sample sizes, since the latter share draws and would understate the spread. Convergence was checked from base sample sizes of 128 to 2048.

Table 1. Model variables, their units, and the conditions imposed at the boundaries of the domain. The depositional flux *F* cancels between the numerator and the denominator of Eq. (5), so no result depends on it. The base condition given is the one the finite-volume solver imposes; the independent collocation solve of Sect. 2.5 instead sets $C_k \rightarrow 0$ at depth, which is adequate there because that check is run per component rather than over the continuum.

Symbol	Description	Unit	Surface condition	Base condition
C_k	mass of reactivity component *k* per unit bed volume and unit *k*	g C cm^{-3} yr	prescribed flux, $F\, g(k) = (w - D_b\lambda_k)C_k(0)$	$dC_k/dz = \lambda_k C_k$
C_0	mass of the inert component, $k = 0$, per unit bed volume	g C cm^{-3}	prescribed flux, $F\, P(\nu, a\, k_{\min})$	advective, $C_0 = F\, P/w$
$g(k)$	deposited mass density over rate constants, Eq. (1)	yr	normalised to unit mass on $(0, \infty)$	none
λ_k	decaying root of the characteristic equation, Eq. (3)	cm^{-1}	none	none
k_{dist}	mass-weighted rate constant of the disturbed layer, Eq. (5)	yr^{-1}	derived	none
z	depth below the sediment-water interface	cm	$z = 0$	$z = L$
φ	porosity, constant except in the compaction scenario	dimensionless	φ_0	φ_∞

Table 1 is the notation key for the whole paper. Each component has its own concentration C_k and its own decay rate *k*, but all components share the same *w* and D_b: the bed moves and mixes every component in the same way, and only the decay term distinguishes them. The inert component C_0 is listed separately because it is the one component that never reacts, so it adds mass to the denominator of Eq. (5) and nothing to the numerator.

Table 2. Environmental and gear parameters, with the reference values used where a single value is required and the ranges over which each is varied. No parameter is fitted.

Symbol	Description	Reference	Range	Unit	Source
w	accumulation rate	0.1	0.02 to 0.6	cm yr^{-1}	northwest European shelf
D_b	biodiffusion coefficient	20	1 to 150	cm^2 yr^{-1}	Middelburg et al. (1997); Solan et al. (2019)
PD	gear penetration depth	2	1 to 5	cm	Pitcher et al. (2022); Khedri et al. (2025)
ν	shape of the deposited continuum	0.15	0.10 to 0.30	dimensionless	Freitas et al. (2021); Pika et al. (2023); Xu et al. (2023)

Symbol	Description	Reference	Range	Unit	Source
a	apparent initial age of the deposit	3	1 to 1000	yr	Freitas et al. (2021); Pika et al. (2023); Xu et al. (2023)
ν/a	mean rate constant of the deposit, closed form	0.05	10^{-4} to 0.3	yr^{-1}	derived from ν and a

Table 2 holds the five parameters of the model. The reference column gives the value used whenever a single number is needed, for example when drawing a profile, and the range column gives the interval swept when the whole shelf is covered. The first three describe the bed and the gear and can be mapped at a site; the last two describe the material settling onto the bed and are fitted from sediment profiles elsewhere. The final row is not an independent parameter but a useful summary: ν/a is the mean decay rate of the material as it arrives, and the results are best read against it.

Table 3. Processes included in the model, the term each contributes to Eq. (2), and where each is relaxed. Processes deliberately omitted are listed at the foot of the table with the section that discusses them.

Process	Term	Treatment in the reference model	Relaxed in
Deposition	$F\,g(k)$ at $z = 0$	steady, one continuum, unit total mass	Sect. 3.2.3, seasonality
Biodiffusive mixing	$d/dz(D_b\, dC_k/dz)$	D_b constant with depth	Sect. 3.2.3, depth-dependent D_b
Burial	$-d(w\, C_k)/dz$	w constant, non-compacting bed	Sect. 3.2.3, compaction
First-order decay	$-k\, C_k$	components decay independently	Sect. 3.4, priming
Non-local transport	$-r(z)C_k$, returned to $z = 0$	absent	Sect. 3.2.3, conveyor
Disturbance	mass-weighted mean over 0 to PD	instantaneous, composition-preserving	Sect. 3.4
Priming, component coupling	none	omitted	Sect. 3.4
Oxygen exposure after disturbance	none	omitted; multiplies the result	Sect. 3.4

Table 3 states what the model does and does not represent. The first four rows are the terms of Eq. (2); the rest are processes that a reader might expect and will not find. The last column is the one to read: most of the simplifications are not left as assumptions but are relaxed and measured in Sect. 3.2.3, and the two that are not, priming and the change in reactivity caused by exposure to oxygen after disturbance, are discussed as limitations in Sect. 3.4.

Table 4. Numerical parameters, and the convergence attained with each. The two solvers are the closed-form quadrature of Eqs. (1) to (6) and the finite-volume discretisation of Sect. 2.4.

Quantity	Value	Convergence attained
Reactivity grid, k_{min} to k_{max}	10^{-14} to 10^{4} yr^{-1}	5×10^{-8} against $k_{min} = 10^{-18}$, over 32 corners of the box

Quantity	Value	Convergence attained
Reactivity grid points	20 000	none
Reactivity grid points, sampling scripts	4000	median 1.7×10^{-7}, maximum 1.9×10^{-6}
Reactivity grid points, depth-dependent solvers	500 to 600	median 1.1×10^{-5}, maximum 1.3×10^{-4}, or 5×10^{-5} decades
Reactivity grid, lognormal continuum	10^{-14} to 10^{12} yr^{-1}, 12 000 points	against 10^{16} yr^{-1}: six figures on the shelf range, 8×10^{-5} relative on the global range
Domain length, L	120 cm	2×10^{-6} over L = 40 to 1200 cm
Nodes, finite-volume solver	6000, dz = 0.02 cm	first order in dz; 3.1×10^{-3} against the closed form
Sobol base sample size	2048	largest change in any index from 512 to 2048 is 0.0013
Sobol scrambles	5, disjoint from the index seed	standard deviation ≤ 0.001 on every index

Table 4 lists every numerical choice together with the error it costs. Each entry answers the same question: if this setting were made finer, how much would the answer move? The largest of these is 3.1×10^{-3} in k_{dist} for the finite-volume solver, and all the others are smaller still. For comparison, the smallest physical effect the paper draws a conclusion from is about 0.08 decades, so no result here is limited by numerics.

Table 5. Sensitivity analyses. Rows are the scenario tested, columns give what was changed and the resulting shift in $\log_{10} k_{dist}$ relative to the reference configuration of Table 2. A positive shift means the departure raises the rate constant of the disturbed layer. ML is the mixed layer and OM is organic matter.

Scenario	Parameter changed	Value	Shift, median (range)
Baseline	nothing changed	D_b constant, non-compacting, steady deposition	0 by definition
Depth-dependent D_b, deep ML	$D_b(z) = ½D_{b,0}[1 - \tanh((z - z_0)/z_s)]$	z_0 = 10 cm, z_s = 2 cm	+0.13 (+0.03 to +0.22)
Depth-dependent D_b, shallow ML	as above	z_0 = 5 cm, z_s = 2 cm	+0.22 (+0.08 to +0.33)
Compaction, matching w at depth	$\varphi(z) = \varphi_\infty + (\varphi_0 - \varphi_\infty)e^{-z/\beta}$	$\varphi_0 = 0.85$, $\varphi_\infty = 0.70$, β = 5 cm	+0.08 (+0.05 to +0.12)
Compaction, matching w at the surface	as above	as above	−0.12 (−0.06 to −0.16)
Conveyor added to biodiffusion	$r(z)$ over a feeding zone, egested at $z = 0$	z_{inj} = 10 cm, $r_0 = D_b/z_{inj}^2$	−0.07 (−0.04 to −0.07)
Conveyor replacing biodiffusion	$D_b = 0$, conveyor only	z_{inj} = 10 cm, $r_0 = 10^{-3}$ to 10^{-1} yr^{-1}	+0.48 to −2.44
Lognormal continuum, shelf	$g(k)$ form, after Xu et al. (2023)	median k 10^{-3} to 10^{-1} yr^{-1}, σ 1 to 3	indices, Sect. 3.2.3

Scenario	Parameter changed	Value	Shift, median (range)
Lognormal continuum, global	as above	median k 10^{-6} to 10^{2} yr^{-1}, σ 0.2 to 6, the whole range in Fig. 7 of Xu et al. (2023) including their soil and incubation data	indices, Sect. 3.2.3
Widened parameter ranges	all five parameters	ν 0.05 to 0.60, a 0.1 to 10^{5} yr, w 0.001 to 2 cm yr^{-1}, D_b 0.01 to 1000 cm^2 yr^{-1}, PD 0.1 to 20 cm	indices, Sect. 3.2.3
Seasonal OM supply	$F(t) = F_0[1 + A \cos \omega t]$	A = 0.5 to 1.0, period 10^{-2} to 10^{6} yr	swing 0.05 to 0.09 at one year

Table 5 sets out the sensitivity analyses. Each row changes one thing about the reference model of Table 2 and reports how far k_{dist} moves as a result, in decades. Rows with a single number pair give a median and the range over the cases tested; the last four rows change the shape of the problem rather than a single value, so their results are reported in Sect. 3.2.3 rather than as one shift. Reading down the shift column, every departure except the substitution of a conveyor for biodiffusion moves the answer by less than a quarter of a decade.

3 Results and discussion

3.1 Baseline profiles and verification of the solution

Figure 1 shows the model. Carbon reaches the seabed as a mixture of reactivities. Bioturbation mixes it downward, burial carries it away from the interface, and each component decays at its own rate. A gear penetrating to depth PD disturbs everything above that depth.

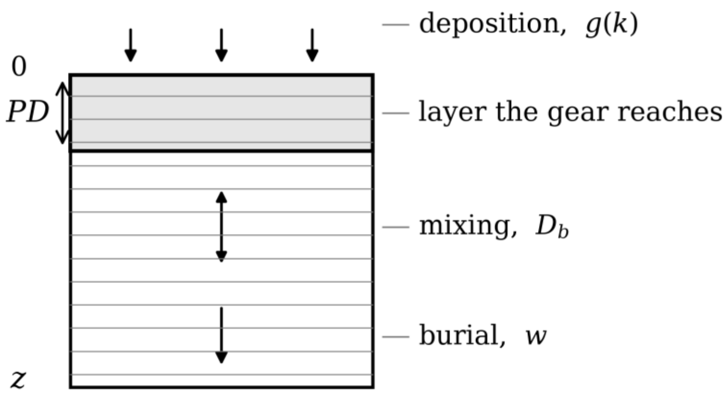

Figure 1. *Sketch of the model. Carbon arrives at the seabed as a mixture of reactivities, is mixed by bioturbation, and is buried. The shaded band is the layer that a gear penetrating to depth PD disturbs.*

Figure 2 shows the steady-state profiles for three mixing intensities. Carbon and reactivity behave quite differently with depth.

The total organic carbon barely changes. It falls by 28 % over the top 25 cm at weak mixing and by 2 % at strong mixing (Fig. 2a), because most of it is refractory and survives that distance whatever the bed does. The bulk rate constant falls much further, by 1.3 decades at weak mixing and 0.3 decades at strong mixing (Fig. 2b), and the volumetric rate falls faster still (Fig. 2c). The fraction of carbon in components that turn over within a century, meaning $k > 10^{-2}$ yr^{-1}, is 0.18 at the sediment surface at weak mixing and 0.035 at strong mixing (Fig. 2d).

Mixing acts in two directions at once. It carries reactive material down, raising the rate constant at depth, and brings old material up, lowering it near the surface. Kuderer and Middelburg (2024) report the same behaviour from particle tracking. The layer a gear reaches lies in the top few centimetres, where the profiles are steepest at weak mixing and nearly flat at strong mixing.

The surface value in Fig. 2b is the plateau of Fig. 5, and reproduces the $PD \rightarrow 0$ limit of Eq. (5) to 1.7×10^{-10}. That is arithmetic, not verification, since both routes evaluate the same expression. It confirms only that the panel plots a rate constant rather than a volumetric rate.

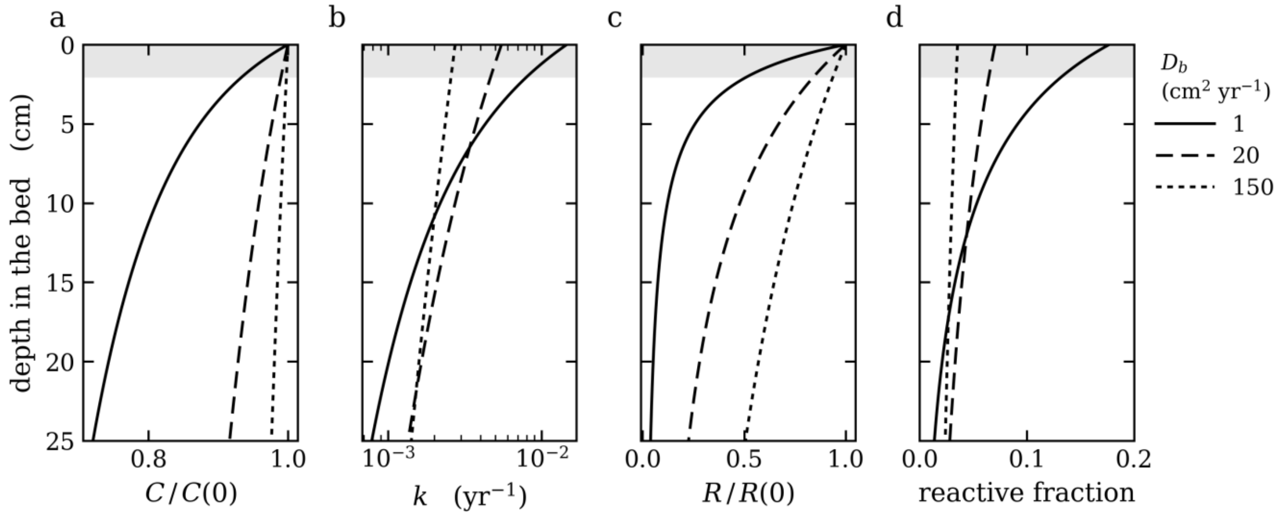

Figure 2. *Depth profiles at steady state for three mixing intensities, at an accumulation rate of 0.1 cm yr^{-1}. Depth increases downward in every panel. (a) Total organic carbon, divided by its value at the sediment surface. (b) Bulk rate constant, that is, the volumetric mineralisation rate divided by the carbon present. (c) Volumetric mineralisation rate, divided by its surface value. (d) Fraction of the carbon held in components with $k > 10^{-2}$ yr^{-1}, which turn over within a century. Panels (a), (b) and (d) include the nearly inert component of Sect. 2.4, which carries mass but does not react. The shaded band is the layer a gear penetrating 2 cm would disturb. Line style marks the biodiffusion coefficient, given in the key.*

The solution was then verified. Over 108 combinations of accumulation rate, mixing, penetration depth and reactivity component, the exponent of Eq. (3) satisfies the governing equation to 4.1×10^{-14}. The depth integral of Eq. (6) matches an independent collocation solve to a median of 1.8×10^{-10}, worst case 1.3×10^{-5} (Fig. 3). That worst case is set by the tolerance of the reference solve, not by the closed form. No case was discarded.

That test treats one component at a time, so it reaches neither the quadrature over the continuum nor the nearly inert fraction that dominates the denominator of Eq. (5). Both are covered by the finite-volume solver, which assembles k_{dist} itself and agrees to 3.1×10^{-3}. That residual halves when the grid spacing halves, as discretisation error should. The two routes share only the local decay exponent, and only in the far-field boundary condition; the quadrature, the flux condition and the depth integration are independent.

Supporting figures follow the same argument. The arriving mixture is plotted in Fig. S1, and the response of k_{dist} to each parameter in turn in Figs. S2 and S3, which recovers the ordering of Sect. 3.2.2 without any sampling.

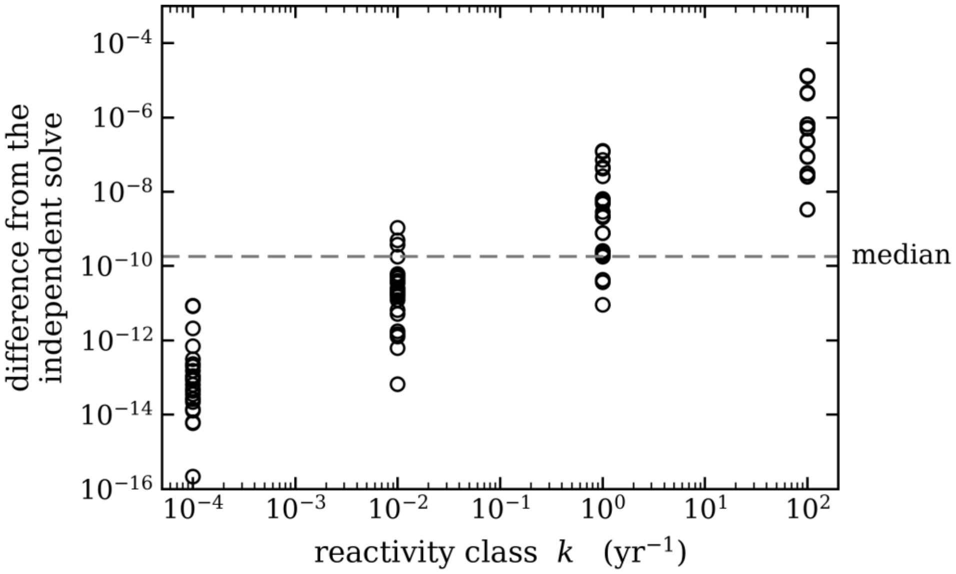

Figure 3. *Check of the closed-form depth integral of Eq. (6) against an independent collocation solve of Eq. (2). Each point is one of 108 combinations of accumulation rate, mixing, penetration depth and reactivity component. The horizontal axis is the reactivity component k, in yr*$^{-1}$*, and the vertical axis is the relative difference between the two solutions. Four values of k were tested, so the points fall in four columns. The grey dashed line marks the median, 1.8 ×* 10^{-10}.

3.2 The rate constant across shelf conditions

Figure 4 maps k_{dist} over accumulation rate and biodiffusion at a penetration depth of 2 cm, with the arriving mixture held at ν = 0.15 and *a* = 3 yr. The rate constant rises with accumulation, because faster burial leaves material less time in the bed before the gear reaches it, and falls with mixing, because mixing dilutes the disturbed layer with older material from below.

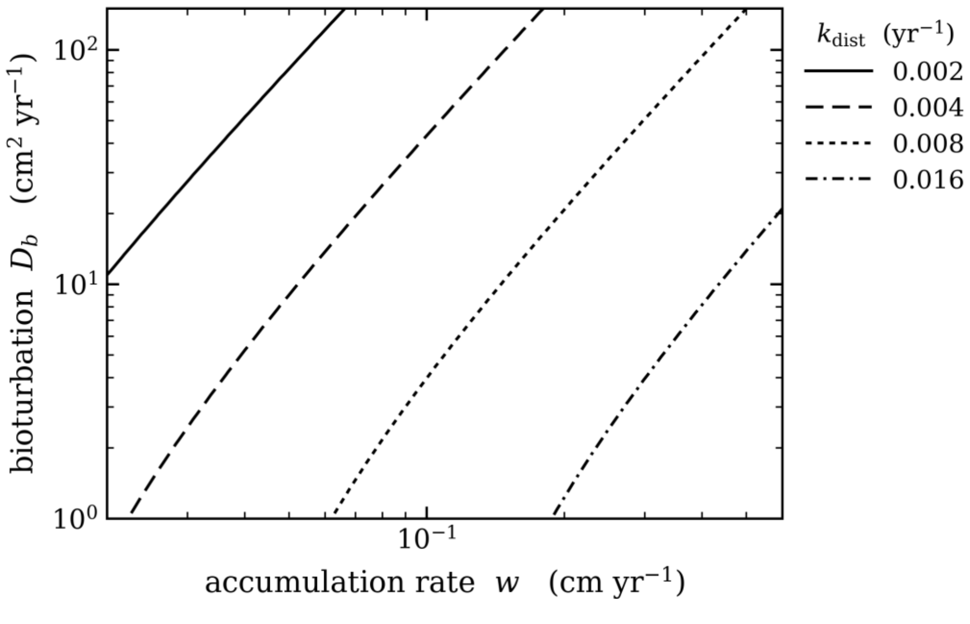

Figure 4. *Contours of the bulk rate constant of the disturbed layer, in yr*$^{-1}$*, over accumulation rate and biodiffusion. Contour values are listed in the key at the right. The penetration depth is 2 cm and the deposited continuum is held at ν = 0.15 and a = 3 yr.*

Over the full shelf ranges of the three transport and gear parameters in Table 2, with the mixture held fixed, k_{dist} runs from 8.3×10^{-4} to 3.2×10^{-2} yr^{-1}: a span of 1.59 decades, median 5.5×10^{-3} yr^{-1}. That median lies within a factor of two of the 10^{-2} yr^{-1} that Khedri et al. (2025) identify as the peak of the published distribution. The model therefore does not move the central estimate. It narrows the range around it and makes the value a function of mappable quantities.

A partial check is available, because the arriving mixture can be taken from an inversion this study did not perform. Xu et al. (2023) report apparent bulk reactivities of about 10^{-2} to 3×10^{-2} yr^{-1} for Arctic shelf regions. Read as the mean rate constant of the arriving material and fed into Eq. (5) at the reference bed of Table 2, those return k_{dist} of 1.8×10^{-3} to 3.7×10^{-3} yr^{-1}, with suppression factors of 5.5 and 8.2.

Three routes to the same quantity are now in hand: the sweep above, at a median of 5.5×10^{-3} yr^{-1}; this one; and the published peak of 10^{-2} yr^{-1} from Khedri et al. (2025). All three lie within three-quarters of a decade of one another, against a computed spread of 4.11 decades when nothing is known about the site. The check is not fully independent, for the reason given in Sect. 3.3: the inversion is run on bed profiles, which are already depleted in reactive components. It is reported because it uses different data, a different functional form and different priors, not because it escapes that bias.

No single reduction factor is quoted against the range currently sampled, for two reasons. That range is ambiguous: the main text of Khedri et al. (2025) gives 10^{-4} to 10^{1} yr^{-1} for the undisturbed rate constant, while their Table 2 gives 10^{-4} to 10^{-1} with a disturbance multiplier of one to five. And the comparison would not be like for like, because 1.59 decades assumes the arriving mixture is known. Section 3.2.2 gives the range without that assumption.

3.2.1 Suppression relative to freshly deposited material

Figure 5 shows the same quantity against penetration depth alone, extended well past the depth any gear reaches. As penetration depth goes to zero the curve settles onto a plateau, and that plateau lies below the mean rate constant of the arriving material. Equation (4) explains why: a component with a large rate constant is consumed within a short distance of the interface and never builds up a standing stock. The bed is therefore already depleted in reactive components at its very top, and gear that scrapes only the topmost millimetre does not meet fresh reactivity.

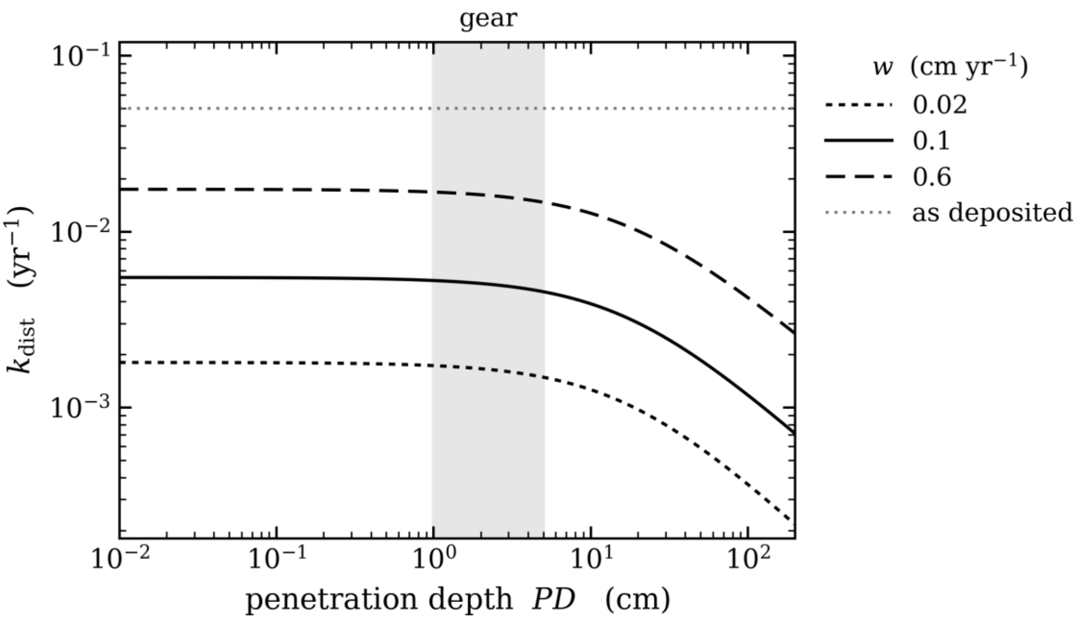

Figure 5. *Bulk rate constant of the disturbed layer against penetration depth, for three accumulation rates at $D_b = 20$ cm^2 yr^{-1}. Accumulation rates are given in the key. The grey dotted line, last in the key, is the mean rate constant of the material as it is deposited, v/a. The shaded band is the range of penetration depths reached by real gear. All three curves lie below the dotted line everywhere, which is the suppression discussed in the text.*

The size of that suppression is not fixed, and the algebra says what sets it. Substituting Eq. (3) into Eq. (4) gives $w - D_b\lambda_k = ½(w + (w^2 + 4D_bk)^{1/2})$, so the standing stock of each component is its deposited mass divided by $½w[1 + (1 + 4D_bk/w^2)^{1/2}]$.

In the limit of a vanishingly thin cut, w cancels between the numerator and the denominator of Eq. (5) and only the dimensionless group D_bk/w^2 survives. The arriving mixture is centred on $k \approx \nu/a$, so the suppression at the sediment surface is a function of ν and $D_b/(a\ w^2)$ alone. At a fixed mixture that reduces to a function of D_b/w^2, which runs from 2.8 to 3.8×10^5 yr over the shelf ranges, and the suppression rises with it throughout. Two qualifications follow. Once the mixture varies, the age enters and the group to hold fixed is $D_b/(a\ w^2)$. For a cut of finite thickness a second group, $k\ PD/w$, enters as well, which is why the reference bed gives 9.1 at the surface and 9.9 over 2 cm.

Varying accumulation and mixing at the fixed mixture of Fig. 4, the suppression factor runs from 1.4 at high accumulation with weak mixing to 56 at the opposite corner, and is 9.1 at the reference bed of Table 2 (Fig. S5a). Varying the mixture as well, over ν, a, w and D_b, it spans 1.0 to 131; penetration depth does not enter, because this is the surface value. Two limits follow from the algebra and are confirmed numerically in Sect. S1. As $D_b \to 0$ the factor tends to one, because an unmixed bed inherits the depositional composition exactly. As $w \to 0$ it grows without bound.

This bears directly on the constant chosen by Sala et al. (2021). In muddy, well-mixed sediments a value taken from fresh deposition overstates the reactivity of the surface standing stock by about an order of magnitude, before penetration depth is considered at all; in rapidly accumulating, weakly mixed sediments the overstatement falls to about 40 %. One condition applies. Sala et al. (2021) already assign a labile fraction of 0.04 to 0.7 by sediment type, which absorbs part of this factor. What is quantified here is the remainder, and how it varies with the bed.

Two published corrections are of the same size. Porz et al. (2024) obtain 4.0 t CO_2 km^{-2} yr^{-1} against the 118 t CO_2 km^{-2} yr^{-1} of Sala et al. (2021), a factor of 30, and Zhang et al. (2024) obtain a global figure below a tenth of the same source. Both reach those factors by running a coupled three-dimensional model of the North Sea, and both attribute them to processes this study does not represent: redeposition of resuspended carbon, the response of the benthic fauna, and the treatment of lightly trawled ground. They are consistent in magnitude with the suppression reported here rather than evidence for it. What the suppression adds is that a factor of this size already follows from the depth profile, and can be written down from Eq. (4) instead of simulated.

Read through this model, Sala et al. (2021) and Hiddink et al. (2023) are disagreeing about which depth interval the rate constant should describe. A fresh-deposit value corresponds to the top of Fig. 2b, a bulk sediment value to well below the disturbed layer. Neither is right, and the right value is not simply between them, because where it falls depends on accumulation and mixing. Figure 4 supplies it wherever those two are mapped.

3.2.2 Where the spread comes from

The span of 1.59 decades assumes the arriving mixture is known. Letting ν and a vary over the ranges of Table 2 as well widens it to 4.11 decades, from 1.1×10^{-5} to 1.5×10^{-1} yr^{-1}, median 2.1×10^{-3} yr^{-1}. That wider figure is the one to compare against a range sampled with no site knowledge at all.

Figure 6 shows where that spread comes from. Each bar is the share one parameter accounts for, computed as in Sect. 2.5.

The apparent initial age of the arriving material carries 0.792 ± 0.001. Accumulation rate carries 0.105, continuum shape 0.068, biodiffusion 0.043 and penetration depth 0.001. Grouped, the two parameters describing the arriving material carry 0.86 against 0.15 for the three describing the bed and the gear. The quoted uncertainty is the standard deviation over five independent scrambles at the same base sample size of 2048, none of them the scramble used for the index itself. The first-order indices sum to 0.993, so the model is close to additive and interactions are weak.

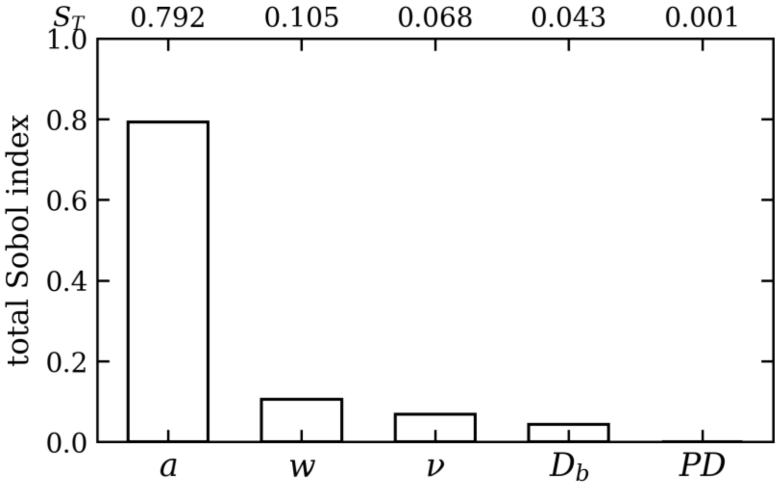

Figure 6. *Share of the spread in $\log_{10} k_{dist}$ accounted for by each parameter, over the ranges of Table 2. The shares are total Sobol indices, so a parameter's bar includes everything it contributes through interactions with the others. The parameters are the apparent initial age a, the accumulation rate w, the continuum shape ν, the biodiffusion coefficient D_b and the penetration depth PD. Each index is printed above its bar. The base sample size is 2048 on a scrambled Sobol' sequence; convergence with sample size is shown in Fig. S4.*

The result for penetration depth is easy to misread. It governs how much carbon is disturbed, and that term is large and well established. Figure 6 says only that it does not govern how reactive the disturbed carbon is. The two enter a trawling estimate as a product, and only the second is insensitive to the gear.

The ordering does not depend on the measure. Repeating the split on k_{dist} itself rather than on its logarithm, at the same sample size, leaves the ranking $a > w > \nu > D_b > PD$ unchanged, though the values move: penetration depth rises from 0.001 to 0.009 and accumulation from 0.105 to 0.285. The logarithmic measure is used because the quantity spans decades and the assessments that consume it sample it log-uniformly. Any single index should be read as belonging to a measure.

3.2.3 Sensitivity analyses

Seven assumptions were tested rather than asserted. Table 5 lists the scenarios; Fig. S5b collects the three signed shifts that share an axis.

The solver. With the radiation condition of Sect. 2.4, the finite-volume solve reproduces the closed form of Eqs. (3) to (6) to 3.1×10^{-3} over five widely separated beds, the worst at the slowest accumulation and weakest mixing. The residual is first-order discretisation error: refining the grid at the reference bed takes it from 3.2×10^{-3} at a spacing of 0.08 cm to 2.0×10^{-4} at 0.005 cm.

What matters more is that it does not depend on domain depth. Over domains from 40 to 1200 cm, k_{dist} agrees to 2×10^{-6}, whereas fixing the concentration to zero at 80 cm overstates it by a factor of 2 to 11. The depth-dependent solver is checked separately by pushing the taper out of the way so that mixing is constant and the answer is known; it agrees to 7.6×10^{-4}. Every budget is checked component by component: deposition equals decay plus burial to the same accuracy, and the conveyor below meets the same budget once ingestion and egestion are set against each other.

Depth-dependent biodiffusion. Replacing constant D_b by the form of Kuderer and Middelburg (2024) raises k_{dist} by 0.03 to 0.22 decades at $z_0 = 10$ cm and by 0.08 to 0.33 decades at $z_0 = 5$ cm. In the first case the cause is not the base of the gear, since $D_b(z)$ is within one per cent of $D_{b,0}$ over the whole top 5 cm. It is that constant biodiffusion on an unbounded domain mixes nearly inert material upward from arbitrarily deep, loading the disturbed layer with refractory carbon and biasing k_{dist} low. At z_0 = 5 cm the taper does reach into the disturbed layer, where D_b has halved, which is part of why the shift is larger.

Compaction. Equation (2) is written for a bed that does not compact. Imposing the porosity profile of Table 5 fixes the product of solid fraction and solid velocity, but not its value, so the sign of the answer turns on which depth the tabulated accumulation rate is taken to describe. Matching the deep solid velocity makes the solid move faster than the reference through the disturbed layer and raises k_{dist} by a median of 0.08 decades, at most 0.12. Matching the velocity at the sediment surface lowers it by a median of 0.12 decades, at most 0.16. Nothing reported with a shelf accumulation rate distinguishes the two conventions, so the honest statement is that compaction moves the answer by less than 0.17 decades, with a sign set by convention rather than by the bed.

Non-local mixing. Meysman et al. (2010) set out where biodiffusion fails, chiefly in beds worked by head-down deposit feeders. Such an animal ingests particles at depth and egests them at the sediment surface, so the operator must remove material at depth and return all of it to the interface (Boudreau, 1986b). Adding that conveyor to biodiffusion, over a 10 cm feeding zone and at an exchange rate matching the mixed-layer turnover time, lowers k_{dist} by 0.04 to 0.07 decades. The sign is the opposite of what an operator injecting material at depth would give: returning carbon to the surface holds it in the disturbed layer for longer, so more of the reactive fraction is gone when a gear arrives.

This is the one result the production grid does not resolve. Recycling a particle 25 to 190 times amplifies the discretisation error by the same factor, and the amplification differs between components, so it does not cancel in a ratio. Each case was therefore run on two grids and extrapolated to zero spacing. The values quoted are the extrapolated ones, within 0.007 decades of the finer grid.

Replacing biodiffusion by the conveyor is a larger change, and it is reported as a sweep rather than at one matched rate, because no exchange rate makes the two closures equivalent. Under biodiffusion a particle can leave the mixed layer by random walk as well as by burial. Under a conveyor it can leave only by burial, after crossing the whole feeding zone without being ingested. Over exchange rates from 10^{-3} to 10^{-1} yr^{-1}, the substitution moves k_{dist} from +0.48 to −2.44 decades, and changes its sign at 0.019 yr^{-1} (Fig. S6). Varying the magnitude of D_b across its whole shelf range, by comparison, moves k_{dist} by 0.61 decades, from −0.28 to +0.33 about the reference bed, and never changes its sign. The shape of the mixing operator therefore matters more than its magnitude. The small total index of D_b in Sect. 3.2.2 cannot show this, because that index varies a coefficient inside one family of closures. This is the largest sensitivity in the study that is not a parameter. At the top of the sweep it is the idealisation that fails, not the arithmetic: a perfect conveyor at 0.2 yr^{-1} recycles a particle 5×10^8 times, which no real bed does, and it is exactly that leakage which biodiffusion represents.

The form of the deposited continuum. Replacing the gamma continuum by the lognormal form fitted globally by Xu et al. (2023), over the shelf ranges those authors report, gives total indices of 0.92 and 0.03 for the two deposit parameters, against 0.062, 0.013 and 0.004 for accumulation, biodiffusion and penetration depth. The deposit again carries almost all of the variance. Over the full range plotted by Xu et al. (2023), which extends beyond their 123 marine sites to the soil and laboratory incubation data they compare with, the indices are 0.98 and 0.10 against 0.014, 0.004 and 0.002. Their marine sites alone sit below a median of 1 yr^{-1}, so this is a deliberate over-widening rather than a marine range. The global case requires the extended reactivity grid of Table 4. Unlike the gamma continuum, a lognormal with a high median and a wide width places real mass above 10^4 yr^{-1}. That mass has a negligible standing stock, but its contribution to the numerator of Eq. (5) is not negligible, and truncating there changes k_{dist} by 43 % at the worst corner.

Seasonality. Everything above is computed at steady state, and shelf deposition is not steady. The model is linear, so a deposition flux varying as $1 + A \cos \omega t$ separates exactly. The mean obeys the balance already solved. The harmonic obeys the same equation with k replaced by $k + i\omega$. Every closed form in Sect. 2 therefore extends to the periodic case with no new machinery and no time stepping.

Figure 7 shows the result. An annual cycle of amplitude 0.8 swings k_{dist} by 0.075 decades at moderate mixing, and an amplitude of one gives 0.093 (Fig. 7a). At strong mixing an amplitude of 0.8 also gives 0.093 (Table 5).

The seasonal signal is confined to the top few centimetres. Over the year, the bulk rate constant spans 23 % of its annual mean at the sediment surface, 6.5 % at 4 cm and 0.9 % at 10 cm (Fig. 7c). The carbon moves far less: 2.9 % at the surface and 0.06 % at 10 cm (Fig. 7b), because most of it is refractory and does not follow the season at all. The extremes of the response do not coincide with the extremes of the supply. At the surface the rate constant peaks 0.12 yr after peak deposition and reaches its minimum 0.62 yr after, and it is 26 % higher at that maximum than at that minimum. Those are full annual ranges. The four times drawn in Fig. 7b and c are equally spaced through the year and miss the extremes, so the panels show less: 17 % rather than 23 % at the surface for the rate constant, and 2.1 % rather than 2.9 % for the carbon.

The swing in k_{dist} is small, and the obvious explanation for that is wrong, so the right one is worth stating. It is not that the numerator and the denominator move together. At one cycle per year, the numerator of Eq. (5) varies by 9.5 % of its mean and the denominator by 1.0 %. The reason is that the numerator is itself damped. The components that supply it have rate constants of order ν/a or below, so their lifetimes exceed a year, and they cannot follow an annual forcing.

The same reasoning explains why the swing is not monotonic in the period of the forcing (Fig. S7). It vanishes for very fast cycles, which the bed filters out, and for very slow ones, which are quasi-steady and to which a ratio is indifferent. In between, the reactive components track the forcing while the refractory reservoir below the disturbed layer cannot, and the swing peaks near 0.66 decades at a period of about a thousand years. Steady state is therefore adequate for the seasonal cycle but not for supply varying on decadal to centennial timescales.

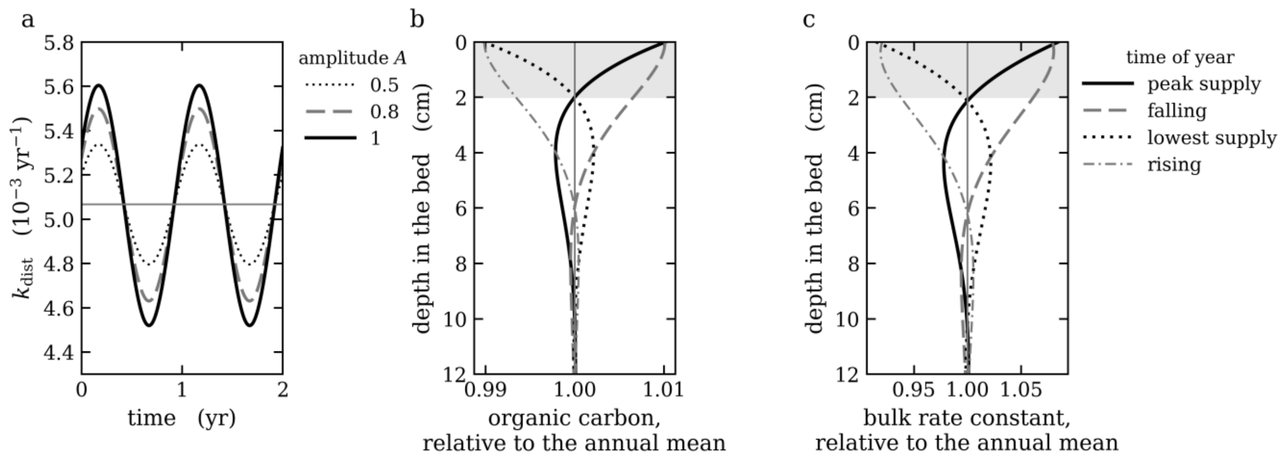

Figure 7. The reference bed under a deposition flux that varies through the year as $F[1 + A \cos \omega t]$, with a period of one year. (a) k_{dist} over two years, for three amplitudes given in the key; the thin grey horizontal line is the steady value. (b) Organic carbon and (c) bulk rate constant against depth, at four equally spaced times in the year, each divided by its own annual mean at the same depth, for $A = 0.8$. The two extremes of the year are drawn in black, solid for peak supply and dotted for lowest supply; the two intermediate phases are drawn in grey. The thin grey vertical line marks the annual mean and the shaded band is the disturbed layer.

The parameter ranges. Widening every range far beyond any defensible shelf box, as set out in Table 5, gives total indices of 0.830 for the apparent initial age, 0.106 for the continuum shape, 0.080 for accumulation, 0.019 for biodiffusion and 0.005 for penetration depth. Only continuum shape and accumulation exchange places. Penetration depth remains last, and remains negligible.

3.2.4 Comparison with process models of trawling

The three process models of trawling and sediment carbon closest to this one all represent organic matter as a small number of discrete pools with prescribed decay constants: two pools in De Borger et al. (2021) and three in Porz et al. (2024) and Zhang et al. (2024). None of them uses a reactivity continuum. The differences below are therefore structural rather than numerical.

The decline of reactivity with depth. Zhang et al. (2024) impose $k(z) = k(0)\ \exp(-0.3\ z)$, with z in cm, below the oxygen penetration depth: 3.26 decades over the top 25 cm. The decline derived here is 1.27 decades at weak mixing, 0.61 at moderate and 0.28 at strong, or e-folding rates of 0.117, 0.056 and 0.026 cm^{-1} (Fig. 2b). The imposed profile is 2.6 to 11 times steeper.

The two are not competing estimates of one quantity and should not be reconciled by adjusting either. Their exponential stands for the loss of microbial activity as oxygen runs out; the decline here comes from composition, the reactive components having already been consumed. Where both act, the total decline is steeper than either alone.

A discrete model does produce some decline unaided, because the labile pools are consumed first, but that decline stops once they are gone and the bulk rate constant is then pinned to the slowest pool. An imposed exponential is what carries the profile past that point. A continuum needs no such device, because a slower component is always still being consumed. That is also why the imposed rate is one number for the whole North Sea, while the derived rate changes by a factor of 4.5 across the mixing range alone.

The transport parameters. De Borger et al. (2021) fit biodiffusion and burial at five stations. Converted to the units used here, their biodiffusion coefficients are 3.7×10^{-5} to 0.63 $cm^2\ yr^{-1}$ and their burial velocities 1.1×10^{-4} and 0.11 cm yr^{-1}. Every one of those coefficients falls below the 1 $cm^2\ yr^{-1}$ minimum swept in Table 2, only three of the five fall inside the widened box of Table 5, and the two slowest burial velocities lie below even that.

Part of the conflict is definitional. The range used here is tracer-derived, being particle displacements inferred from ^{210}Pb and ^{234}Th and compiled by Middelburg et al. (1997) and Solan et al. (2019). Theirs is a coefficient fitted inside a two-pool model against measured oxygen and ammonium profiles, where it absorbs everything two pools cannot represent and is fitted jointly with the decay constant of the slow pool, so the two trade off. The quantities share a symbol and are not the same number.

Part of the conflict is real. About a tenth of the shelf records in Solan et al. (2019) also lie below 1 $cm^2\ yr^{-1}$, so the prior used here does not cover every quietly mixed bed. The distinction matters because the suppression factor scales with D_b/w^2, so reading one literature against the other directly would misstate the effect by orders of magnitude.

The direction of the trawling effect. De Borger et al. (2021) report that trawling lowers mineralisation within the sediment, by 5 % to 29 % depending on station and frequency, while Porz et al. (2024) and Zhang et al. (2024) emphasise a net loss driven by resuspension into the water column. These are not in conflict: they refer to different compartments, and the model here sits beneath both because it returns a rate constant rather than a flux. One observation from Zhang et al. (2024) does bear on the profiles. They find that heavily trawled sediment keeps a higher reactivity at depth than untrawled sediment, which is the behaviour Fig. 2b produces from mixing alone.

3.3 Value of a regional constraint on the deposited continuum

With every parameter varied over its full range, the computed spread is 4.11 decades. Knowing the three sediment and gear parameters exactly leaves 2.77 decades. Characterising the gear and the bed therefore removes 1.34 decades.

What a constraint on the arriving material is worth depends on how tight it can be made, which cannot be assumed, so Fig. 8 reports it as a curve. Pinning the apparent initial age to within a quarter of a decade removes 1.81 decades; to within one decade, 1.28; to within two decades, 0.61. The curve crosses the value of knowing the gear and the bed exactly at a residual spread of 0.91 decades.

The constraint in Fig. 8 narrows the apparent initial age and nothing else, which is what makes it comparable with the spread Xu et al. (2023) report for that quantity. Narrowing the shape at the same time is a different and larger claim: it removes 2.31 decades at a quarter of a decade rather than 1.81. Both curves are in the deposited table. An earlier version of this analysis narrowed the shape inside the same calculation without saying so, and credited the age constraint with about half a decade that belonged to the shape.

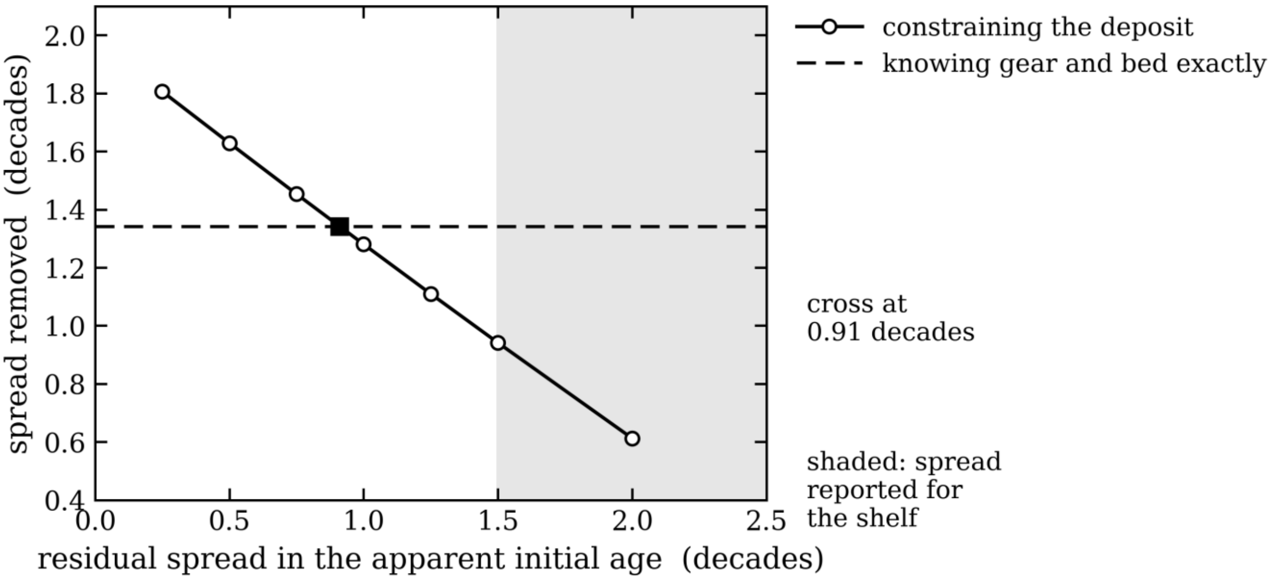

Figure 8. *Decades of spread in $\log_{10} k_{dist}$ removed by constraining the apparent initial age of the deposited material, plotted against how tightly that age is constrained. The horizontal line is the 1.34 decades removed instead by knowing accumulation, biodiffusion and penetration depth exactly, computed independently of the curve. The square marks where the two cross, at a residual spread of 0.91 decades. The shaded band is the spread now reported for shelf sediments, which lies to the right of the crossing.*

That crossing is the practical result, and on present knowledge it falls on the unfavourable side. Xu et al. (2023) report mean reactivities within the shelf group spanning about two decades, and Pika et al. (2023) report regionally averaged rate constants from 8×10^{-5} to 0.27 yr^{-1}, with site-level values spanning far more. An inversion delivering the arriving mixture to two decades would remove 0.61 decades, less than half the 1.34 available from characterising the gear and the bed. Constraining the arriving material is therefore the better investment only below about 0.9 decades, which no published regional inversion approaches.

The threshold is not an artefact of how the calculation is set up. Refining the grid in the apparent initial age from three values to seventeen changes it by less than 0.001 decades. Moving the centre of the constraint from 3 to 100 yr moves it from 0.79 to 1.25, with 1.07 at the geometric centre of the prior range. All of these remain far below the two decades the literature reaches.

This does not weaken the result of Sect. 3.2.2. Which parameter carries the spread and which is cheapest to pin down are different questions. The arriving mixture dominates the spread by six to one and would repay a tight constraint; at the precision now available it cannot be constrained tightly.

The obvious route to that constraint has a difficulty of principle. The global inversions of Xu et al. (2023) are performed on accumulated bed profiles and those of Pika et al. (2023) on diffusive oxygen uptake at the sediment surface. Neither observes the depositing material, and Sect. 3.2.1 shows the surface standing stock is depleted in reactive components relative to the deposit by a factor of 1.4 to 56. An inversion of the bed therefore returns a biased proxy, and using it here would be close to circular.

Two ways out exist. The direct one is to measure the deposit, using an incubation series on sediment-trap material, which returns both continuum parameters without passing through the bed. The indirect one is to correct a bed inversion with the suppression factor of Sect. 3.2.1, which this model already supplies.

3.4 Limitations and challenges

Six limitations bound the result.

Before disturbance only. The model gives the rate constant of the material as the gear arrives. Trawling is thought to raise reactivity by exposing carbon to oxygen, and Khedri et al. (2025) apply a factor of one to five for that. It multiplies the constant computed here and is not addressed, which is the largest gap between what this study delivers and what a trawling budget needs.

Biodiffusion, in two parts. Relaxing constant D_b raises k_{dist} by a median of 0.13 decades, through the unbounded mixing domain rather than the base of the gear. That bias moves the answer back toward Sala et al. (2021), so it works against the argument made here. The second part concerns the closure rather than its coefficient: replacing biodiffusion by a conveyor moves k_{dist} by up to 2.4 decades and can reverse the sign (Sect. 3.2.3), far more than varying D_b across its whole shelf range. For beds worked by head-down deposit feeders, the results give a magnitude and not a value.

One constant for two disturbed masses. Equation (5) takes the mass-weighted mean over the layer the gear reaches. That average holds whether the gear lifts the layer into the water column or homogenises it in place, because the decay rate of a mixture does not change when its parts are rearranged, and the event lasts hours to days while k_{dist} is of order 10^{-3} to 10^{-2} yr^{-1}, so the mixture ages negligibly during it. The inconsistency is elsewhere. Khedri et al. (2025) carry a thin resuspended skim and the full mixed layer with different recovery times, and one $k_{dist}(PD)$ should not serve both. The plateau of Fig. 5 is the right constant for the skim, and it differs from the full-layer value at 2 cm by 3 % at strong mixing and 37 % at weak mixing, so it matters most where the profile is steepest. That difference is governed mainly by D_b and, unlike the suppression factor of Sect. 3.2.1, collapses onto no single group.

Steady state. This is a smaller concession than it sounds. The depositional flux cancels from Eq. (5) only at steady state, because fast components track the instantaneous flux while slow ones integrate the long-term mean. An annual cycle of amplitude 0.8 swings k_{dist} by at most 0.093 decades, fourteen times smaller than the 1.34 decades on which Sect. 3.3 turns. Longer periods are different: a cycle of decades to centuries moves k_{dist} by up to half a decade (Fig. S7). A shelf whose supply has changed over the last century falls outside this description; a shelf with a strong spring bloom does not.

No confrontation with observation. Bartl and Thrush (2025) report resuspension-induced CO_2 production at 57 sites in the Hauraki Gulf, the closest existing measurement of this process, but a site-by-site test is not possible: they report organic matter content, coarse-sand fraction and water depth, while the model needs accumulation rate, biodiffusion, penetration depth and the two continuum parameters.

Two weaker tests remain. The first is ordinal. Over the whole shelf box k_{dist} rises with accumulation at fixed mixing in all 1440 adjacent pairs tested, and falls with mixing at fixed accumulation in 1438 of them; the two exceptions sit at the freshest deposit with the deepest cut and the weakest mixing, where mixing carries reactive material down into a layer already reaching well below the surface. Binning those 57 sites by published sedimentation rates and mixing depths would give a predicted ordering to confirm or refute. The second is direct. The suppression factor of 1.4 to 56 is the sharpest claim made here, and an incubation series on sediment-trap material against surface sediment from the same site would test it. No such paired dataset is known to the author, and producing one would settle the mechanism faster than further modelling.

An instantaneous mean. Equation (5) gives the rate at the moment of disturbance, and a budget applies it over a recovery time. Because the mixture is not exponential, its apparent rate falls as the reactive components are used up: at the reference bed the constant reproducing the cumulative loss is 1.7 times smaller than k_{dist} over ten years and 4.8 times smaller over a century. A one-pool model fed k_{dist} therefore overstates cumulative mineralisation on those timescales, by about as much as the suppression factor understates the initial rate. A budget running for decades needs the whole mixture, not its mean.

Independent components. The components are assumed to decay independently, which is what a continuum description means. Priming violates that assumption, and there is recent evidence for it in marine sediments (Zhu et al., 2024). Coupling the components would change the indices but not their ordering, because the apparent initial age acts by shifting the whole mixture along the reactivity axis, and priming modifies that shift rather than removing it.

3.5 Potential impact on trawling carbon budgets

The result carries a recommendation that runs against current practice. Khedri et al. (2025) call for experiments on how disturbance alters reactivity. Those are worth doing, but Fig. 6 shows the leverage lies elsewhere: the dominant term is the apparent initial age of the depositing material, a property of the supply rather than of the disturbance. One condition attaches, from Sect. 3.3. A regional constraint must reach better than 0.91 decades before it beats characterising the gear and the bed.

Tiano and De Borger (2026) argue from a synthesis of the observations that the carbon consequences of trawling depend on the depositional setting and on how degradable the arriving material is, and that management should be habitat-specific. Their argument is qualitative, made with a conceptual diagram of lability against deposition rate. The results here quantify one half of it: how degradable the arriving material is accounts for 0.86 of the spread, the strongest possible version of their first axis. Their conclusion nevertheless differs from the one drawn here. They would prioritise beds with high burial efficiency even where the carbon is unreactive, whereas Sect. 3.3 asks only where measurement effort buys the most precision. The two are complementary; neither answers the other's question.

Two adjacent routes already exist. Stolpovsky et al. (2015) prescribe the depth profile of mineralisation through the bioturbated layer globally from the particulate organic carbon rain rate and derive rate constants from it, and a trawling modeller could integrate that profile from the surface to the cutting depth today. The difference is where the depth dependence comes from. Theirs is imposed as a power law and calibrated; here it follows from accumulation, mixing and the composition of what was deposited, so it responds to those without recalibration. Meile and Van Cappellen (2005) set out the underlying difficulty, that particle age depends jointly on burial velocity and mixing rate, which is the dependence Eq. (3) makes explicit.

The title should be read carefully. The rate constant of disturbed material is not eliminated as an unknown; it is moved. It now rests on the two continuum parameters, which carry 0.86 of the spread and describe the material arriving at the seafloor. That material is measurable and already mapped globally. The quantity it replaces, the reactivity of sediment after a trawl has passed, is neither.

4 Conclusions

Estimates of the carbon released when fishing gear is dragged across the seabed all depend on one number: how fast the disturbed carbon breaks down and this number is currently being assumed rather than calculated, and it is the largest single uncertainty in those estimates. This study shows that it can be calculated and three parameters are needed, and each of them can be measured at a site: i. how deep the gear cuts, ii. how fast sediment builds up, and iii. how strongly animals mix the bed. Given those three, the rate constant can be written down as a formula, starting from the mixture of reactivities that arrives at the seabed.

That formula was tested against an independent numerical solution, in two stages. Taken one component at a time, the two agree to a median of 1.8×10^{-10}. Taken over the whole mixture, where the sum across components and the almost unreactive part also enter, they agree to 3.1×10^{-3}.

Two ranges follow, and which one applies depends on how much is known about the arriving material. If its reactivity is known, the rate constant varies by 1.59 decades across the conditions found on continental shelves, with a median of 5.5×10^{-3} yr^{-1}. If it is not known, the variation widens to 4.11 decades. Splitting that wider figure according to which input it came from shows where it comes from. The apparent initial age of the arriving material accounts for 0.792 ± 0.001 of it. How deep the gear cuts accounts for 0.001.

A second result is about what a gear can reach at all. Fresh material never builds up at the seabed, because its reactive part is used up just below the sediment surface. Gear that scrapes only the top of the bed therefore lifts material that is already old. Between the reactivity of the arriving material and the reactivity of the sediment surface there is a gap of 1.4 to 56 for a fixed arriving mixture, and of 1.0 to 131 once that mixture is allowed to vary as well. At a fixed arriving mixture the size of that gap is governed by one combination of the transport terms, D_b/w^2, and once the mixture is allowed to vary the age of the material enters too, as $D_b/(a\ w^2)$. The gap closes only in a bed that is not mixed at all.

The reactivity of disturbed carbon is therefore set by what settles on the seabed, not by the gear that disturbs it. That changes what is worth measuring. Of the 4.11 decades of spread, mapping how fast sediment builds up, how strongly it is mixed and how deep the gear cuts removes 1.34, and those three can be mapped with methods that already exist. Working on the arriving material would remove more, but only once its apparent initial age is known to better than 0.91 decades; at the two decades reached so far it removes 0.61. That threshold is the target this study sets for the measurement, and the formula given here converts either kind of progress directly into a rate constant.

Code availability

All computations are implemented in Python and require only numpy and scipy. Sixteen scripts produce every result and figure: fifteen that compute and plot, and one that carries the figure style. They, the tables they write, and all figures will be deposited at Zenodo under a CC-BY licence upon acceptance, and are included with this submission as the Supplement. Every number quoted in the text is printed by one of them; none is computed anywhere else.

Data availability

No measured data were generated and none were used. All parameter ranges are given in Table 2 with their sources. The tables underlying every figure are deposited with the code and included in the Supplement. Sect. 3.4 states why no confrontation with the observational dataset closest to this process was attempted, and what measurement would make one possible.

Supplement

The Supplement contains seven supporting figures (Figs. S1 to S7), the reference implementation of the core routines, the fifteen computation and plotting scripts, and the thirteen tables of results they write.

Author contributions

SA designed the study, carried out the derivations and computations, produced the figures, and wrote the manuscript.

Competing interests

The author declares that he has no conflict of interest.

Acknowledgements

During the preparation of this manuscript the author used a large language model to assist with editing text. The author reviewed and verified all content, results and figures, and takes full responsibility for the work.

Use of Generative Artificial Intelligence

The author used a large language model to edit the manuscript for grammar and readability. The author reviewed and verified all content, results and figures, and takes full responsibility for the work.

References

Arndt, S., Jørgensen, B. B., LaRowe, D. E., Middelburg, J. J., Pancost, R. D., and Regnier, P.: Quantifying the degradation of organic matter in marine sediments: a review and synthesis, Earth-Sci. Rev., 123, 53 to 86, 2013.

Atwood, T. B., Romanou, A., DeVries, T., Lerner, P. E., Mayorga, J. S., Bradley, D., Cabral, R. B., Schmidt, G. A., and Sala, E.: Atmospheric CO2 emissions and ocean acidification from bottom-trawling, Front. Mar. Sci., 10, 1125137, 2024.

Bartl, I. and Thrush, S.: Sediment heterogeneity shapes spatial variability of resuspension-induced CO2 production, Biogeosciences, 22, 7441 to 7454, 2025.

Boudreau, B. P.: Mathematics of tracer mixing in sediments: I. Spatially-dependent, diffusive mixing, Am. J. Sci., 286, 161 to 198, 1986a.

Boudreau, B. P.: Mathematics of tracer mixing in sediments: II. Nonlocal mixing and biological conveyor-belt phenomena, Am. J. Sci., 286, 199 to 238, 1986b.

Boudreau, B. P. and Ruddick, B. R.: On a reactive continuum representation of organic matter diagenesis, Am. J. Sci., 291, 507 to 538, 1991.

De Borger, E., Tiano, J., Braeckman, U., Rijnsdorp, A. D., and Soetaert, K.: Impact of bottom trawling on sediment biogeochemistry: a modelling approach, Biogeosciences, 18, 2539-2557, 2021.

Epstein, G., Middelburg, J. J., Hawkins, J. P., Norris, C. R., and Roberts, C. M.: The impact of mobile demersal fishing on carbon storage in seabed sediments, Glob. Change Biol., 28, 2875 to 2894, 2022.

Freitas, F. S., Pika, P. A., Kasten, S., Jørgensen, B. B., Rassmann, J., Rabouille, C., Thomas, S., Sass, H., Pancost, R. D., and Arndt, S.: New insights into large-scale trends of apparent organic matter reactivity in marine sediments and patterns of benthic carbon transformation, Biogeosciences, 18, 4651 to 4679, 2021.

Hiddink, J. G., van de Velde, S. J., McConnaughey, R. A., De Borger, E., Tiano, J., Kaiser, M. J., Sweetman, A. K., and Sciberras, M.: Quantifying the carbon benefits of ending bottom trawling, Nature, 617, E1-E2, 2023.

Khedri, P., Gourgue, O., Depestele, J., Arndt, S., and van de Velde, S. J.: Reconciling the impact of mobile bottom-contact fishing on marine organic carbon sequestration, ICES J. Mar. Sci., 82, fsaf154, 2025.

Kuderer, M. and Middelburg, J. J.: Organic carbon reaction kinetics in bioturbated sediments, Geophys. Res. Lett., 51, e2024GL110404, 2024.

Meile, C. and Van Cappellen, P.: Particle age distributions and O2 exposure times: timescales in bioturbated sediments, Global Biogeochem. Cy., 19, GB3013, 2005.

Meysman, F. J. R., Boudreau, B. P., and Middelburg, J. J.: Relations between local, nonlocal, discrete and continuous models of bioturbation, J. Mar. Res., 61, 391 to 410, 2003.

Meysman, F. J. R., Boudreau, B. P., and Middelburg, J. J.: When and why does bioturbation lead to diffusive mixing?, J. Mar. Res., 68, 881 to 920, 2010.

Middelburg, J. J.: A simple rate model for organic matter decomposition in marine sediments, Geochim. Cosmochim. Ac., 53, 1577 to 1581, 1989.

Middelburg, J. J., Soetaert, K., and Herman, P. M. J.: Empirical relationships for use in global diagenetic models, Deep-Sea Res. Pt. I, 44, 327 to 344, 1997.

Pika, P. A., Hülse, D., Eglinton, T. I., and Arndt, S.: Regional and global patterns of apparent organic matter reactivity in marine sediments, Global Biogeochem. Cy., 37, e2022GB007636, 2023.

Pitcher, C. R., Hiddink, J. G., Jennings, S., Collie, J., Parma, A. M., Amoroso, R., Mazor, T., Sciberras, M., McConnaughey, R. A., Rijnsdorp, A. D., Kaiser, M. J., Suuronen, P., and Hilborn, R.: Trawl impacts on the relative status of biotic communities of seabed sedimentary habitats in 24 regions worldwide, P. Natl. Acad. Sci. USA, 119, e2109449119, 2022.

Porz, L., Zhang, W., Christiansen, N., Kossack, J., Daewel, U., and Schrum, C.: Quantification and mitigation of bottom-trawling impacts on sedimentary organic carbon stocks in the North Sea, Biogeosciences, 21, 2547-2570, 2024.

Rooze, J., Jung, H., and Radtke, H.: A novel Eulerian model based on central moments to simulate age and reactivity continua interacting with mixing processes, Geosci. Model Dev., 16, 7107 to 7121, 2023.

Sala, E., Mayorga, J., Bradley, D., Cabral, R. B., Atwood, T. B., Auber, A., Cheung, W., Costello, C., Ferretti, F., Friedlander, A. M., Gaines, S. D., Garilao, C., Goodell, W., Halpern, B. S., Hinson, A., Kaschner, K., Kesner-Reyes, K., Leprieur, F., McGowan, J., Morgan, L. E., Mouillot, D., Palacios-Abrantes, J., Possingham, H. P., Rechberger, K. D., Worm, B., and Lubchenco, J.: Protecting the global ocean for biodiversity, food and climate, Nature, 592, 397 to 402, 2021.

Solan, M., Ward, E. R., White, E. L., Hibberd, E. E., Cassidy, C., Schuster, J. M., Hale, R., and Godbold, J. A.: Worldwide measurements of bioturbation intensity, ventilation rate, and the mixing depth of marine sediments, Sci. Data, 6, 58, 2019.

Stolpovsky, K., Dale, A. W., and Wallmann, K.: Toward a parameterization of global-scale organic carbon mineralization kinetics in surface marine sediments, Global Biogeochem. Cy., 29, 812 to 829, 2015.

Tiano, J. C. and De Borger, E.: Rethinking the impacts of bottom trawling on seabed carbon: biogeochemical mechanisms, vulnerability and long-term climate consequences, J. Appl. Ecol., 63, e70346, 2026.

Xu, S., Liu, B., Arndt, S., Kasten, S., and Wu, Z.: Assessing global-scale organic matter reactivity patterns in marine sediments using a lognormal reactive continuum model, Biogeosciences, 20, 2251 to 2263, 2023.

Zhang, W., Porz, L., Yilmaz, R., Wallmann, K., Spiegel, T., Neumann, A., Holtappels, M., Kasten, S., Kuhlmann, J., Ziebarth, N., Taylor, B., Ho-Hagemann, H. T. M., Bockelmann, F. D., Daewel, U., Bernhardt, L., and Schrum, C.: Long-term carbon storage in shelf sea sediments reduced by intensive bottom trawling, Nat. Geosci., 17, 1268-1276, 2024.

Zhu, Q.-Z., Yin, X., Taubner, H., Wendt, J., Friedrich, M. W., Elvert, M., Hinrichs, K.-U., and Middelburg, J. J.: Secondary production and priming reshape the organic matter composition in marine sediments, Sci. Adv., 10, eadm8096, 2024.

Appendix A: Derivation of the displayed equations

A1 The arriving mixture, Eq. (1). A continuum description replaces a few discrete pools by a density $g(k)$ over first-order rate constants, so the mass deposited with rate constant between k and $k + \mathrm{d}k$ is $F\,g(k)\,\mathrm{d}k$. The gamma density of Boudreau and Ruddick (1991) is the standard choice because a mixture drawn from it decays as a power law, which is what sediment profiles show.

Both parameters have direct readings. ν sets how much mass sits in the slowly reacting tail. a sets the reactivity of the mixture as a whole, because a mixture with parameters (ν, a) behaves after time t exactly like a freshly deposited mixture with parameters (ν, $a + t$). That ageing property is why a is called an apparent initial age, and why it dominates the split of Sect. 3.2.2.

A2 The steady balance, Eq. (2). Take one reactivity component. Its mass per unit volume changes through biodiffusive mixing, burial and decay. Bioturbation over these timescales is represented as a diffusive flux $-D_b\,\mathrm{d}C_k/\mathrm{d}z$, burial as a flux $w\,C_k$, and decay removes $k\,C_k$ per unit volume per unit time. Setting the time derivative to zero and subtracting the divergence of the two fluxes gives Eq. (2). Components do not appear in one another's equations, which is the defining assumption of a continuum description; Sect. 3.4 states where it fails.

A3 The profile, Eq. (3). Equation (2) is linear with constant coefficients, so solutions are exponentials $C_k = A\, e^{\lambda z}$ with $D_b\lambda^2 - w\lambda - k = 0$. The two roots are

$$\lambda_\pm = \frac{w \pm \sqrt{w^2 + 4D_b k}}{2D_b}.$$

Since $k > 0$ the square root exceeds w, so $\lambda_+ > 0$ and $\lambda_- < 0$. A profile that does not grow without bound at depth must take the negative root, which is Eq. (3).

Two limits check it. Without mixing, $D_b \to 0$, expanding the root gives $\lambda_- \to -k/w$, so the profile decays over the length w/k, which is burial velocity times lifetime, as it must. Without burial, $w \to 0$, it gives $\lambda_- \to -(k/D_b)^{1/2}$, the classical reaction-diffusion penetration depth.

A4 The surface value, Eq. (4). The flux of component k at depth z is advective plus diffusive, $J_k = w\, C_k - D_b\, \mathrm{d}C_k/\mathrm{d}z$, and at the interface it must equal the depositional supply $F\, g(k)$. Substituting Eq. (3) gives $J_k(0) = (w - D_b\lambda_k)C_k(0)$, and solving for $C_k(0)$ gives Eq. (4). The bracket is positive because λ_k is negative, so the surface concentration is positive for every component.

A5 The disturbed-layer rate constant, Eqs. (5) and (6). A one-pool model assigns one rate constant to a mass of material. The consistent choice is the one that reproduces the instantaneous decay rate of that mass, which is the mass-weighted mean over the components present, Eq. (5). The depth integral is elementary since each component is exponential,

$$\int_0^{PD} C_k\,(0)\, e^{\lambda_k z}\, \mathrm{d}z = C_k(0)\, \frac{e^{\lambda_k PD} - 1}{\lambda_k},$$

which is Eq. (6), and is positive because numerator and denominator are both negative. Substituting Eqs. (4) and (6) into Eq. (5), the depositional flux F cancels between numerator and denominator, so k_{dist} depends only on the shape of the arriving mixture and on w, D_b and PD, not on how much carbon arrives. The magnitude of the flux always cancels; what steady state buys is that k_{dist} then carries no dependence on the shape of the supply either. Section 3.2.3 gives the size of that dependence under a periodic flux.

The limit as $PD \to 0$ deserves care, because the obvious guess is wrong. It is not the flux-weighted mean of what is deposited, ν/a. Equation (4) divides each component by $w - D_b\lambda_k = ½(w + (w^2 + 4D_b k)^{1/2})$, which for fast components grows like $(D_b k)^{1/2}$. Reactive components are therefore under-represented in the standing stock even at the interface, being consumed within a short distance of it and never accumulating. The limit is the concentration-weighted mean of the standing stock at $z = 0$.

The ratio of the two is therefore a function of the parameters, not a constant, and it has two limits. As $D_b \to 0$ the factor $w - D_b\lambda_k \to w$, the same for every component, so the standing stock inherits the depositional composition exactly and the ratio tends to one: numerically 1.030 at $D_b = 10^{-3}$, 1.003 at 10^{-4} and 1.0005 at 10^{-5} cm^2 yr^{-1}. As $w \to 0$ the factor tends to $(D_b\, k)^{1/2}$ and the ratio grows without bound, reaching 1133 at $w = 10^{-4}$ cm yr^{-1}. Between these, over the ranges of Table 2, it runs from 1.4 to 56 and equals 9.1 at the reference bed. As PD grows beyond the penetration depth of every component, the rate constant falls further, toward the mean over the whole accumulated deposit.

A6 The inert component. For $\nu < 1$ the density of Eq. (1) diverges as $k \to 0$, so any finite lower limit $k_{\min}$ omits a mass fraction $P(\nu, a\, k_{\min})$, the regularised lower incomplete gamma. That mass is real and nearly inert, so it must be carried rather than renormalised away. Its profile follows from the $k \to 0$ limit of Eq. (3): $\lambda_k \to -k/w$, so $C_k(0) \to F\, g(k)/w$ and the depth integral of Eq. (6) tends to $C_k(0)\, PD$. It therefore contributes $P(\nu, a\, k_{\min})\, PD/w$ to the denominator of Eq. (5) and nothing to the numerator.

That advective limit is valid when $k_{\min} \ll w^2/(4D_b)$. At the most demanding corner of the box, w = 0.02 cm yr^{-1} and D_b = 150 cm^2 yr^{-1}, the threshold is 6.7×10^{-7} yr^{-1}, so a grid starting at 10^{-6} does not satisfy it and converges only to about three per cent. Referred to a grid extended to 10^{-18} yr^{-1}, the worst deviation over the 32 corners of the box is 2.9 per cent at $k_{\min} = 10^{-6}$, 2.1×10^{-4} at 10^{-8}, 1.2×10^{-6} at 10^{-10} and 5×10^{-8} at the 10^{-14} used here. Six significant figures are reached from 10^{-10} downward.

The alternative is worse. Renormalising the grid to unit mass reassigns the omitted mass to the surviving components and inflates the reactivity of the deposit: at the truncation used here by 1.0 per cent at ν = 0.15, a = 3 yr and 9.1 per cent at ν = 0.10, a = 1000 yr, giving errors in k_{dist} at the reference bed of 2.1 and 9.9 per cent. The penalty grows as the grid is shortened, reaching 8.7 and 50 per cent in the deposit mean at $k_{\min} = 10^{-8}$. Carrying the component costs nothing and removes the question.

S1 Supporting figures

The seven figures below back up statements made in the main text. Each one is named where it is first used, and each is followed by a short note saying what to take from it.

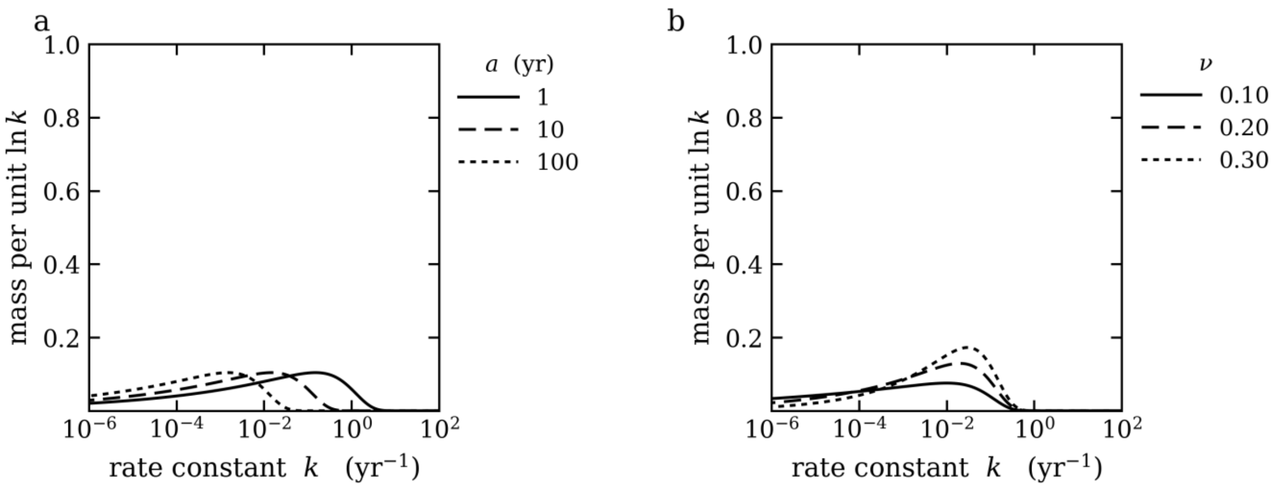

Figure S1. *What the material landing on the seabed looks like when it is sorted by how fast it decays. The horizontal axis is the decay rate constant k, and the vertical axis is how much mass sits at each rate. The vertical axis carries mass per unit ln k, so equal areas mean equal mass. (a) The spread is held fixed and the age of the material is varied. (b) The age is held fixed at 10 yr and the spread is varied.*

The two parameters do different things. Making the material older slides the whole curve to the left, toward slower decay, without changing its width. That is why the age carries most of the spread in k_{dist}. Changing the shape only adds or removes mass in the slow tail. The bulk of the curve stays where it is, so the shape matters much less.

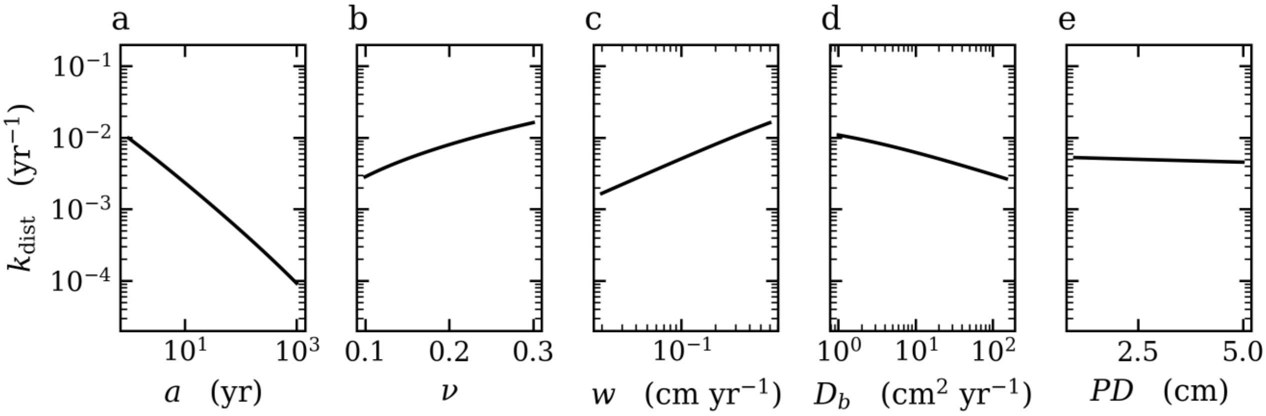

Figure S2. *How much k_{dist} moves when one parameter is changed and the other four are held at their reference values. Panels (a) to (e) are the apparent initial age a, the shape ν, the accumulation rate w, the biodiffusion coefficient D_b and the penetration depth PD. All five use the same vertical scale, so they can be compared by eye.*

Changed on its own, the age of the arriving material moves k_{dist} by 2.03 decades. The other four move it by 0.99 for the accumulation rate, 0.76 for the shape, 0.61 for mixing and 0.06 for the cutting depth. Only the cutting depth is negligible.

The ranking is the same as in Fig. 6 of the main text, but the numbers are not comparable, and the reason is worth stating. Here each parameter is moved on its own, from one starting point. There, each parameter is credited with the share of the whole spread it accounts for when all five move together, and the age is sampled over a wider range than the others. That two different calculations return the same ranking is a check on both.

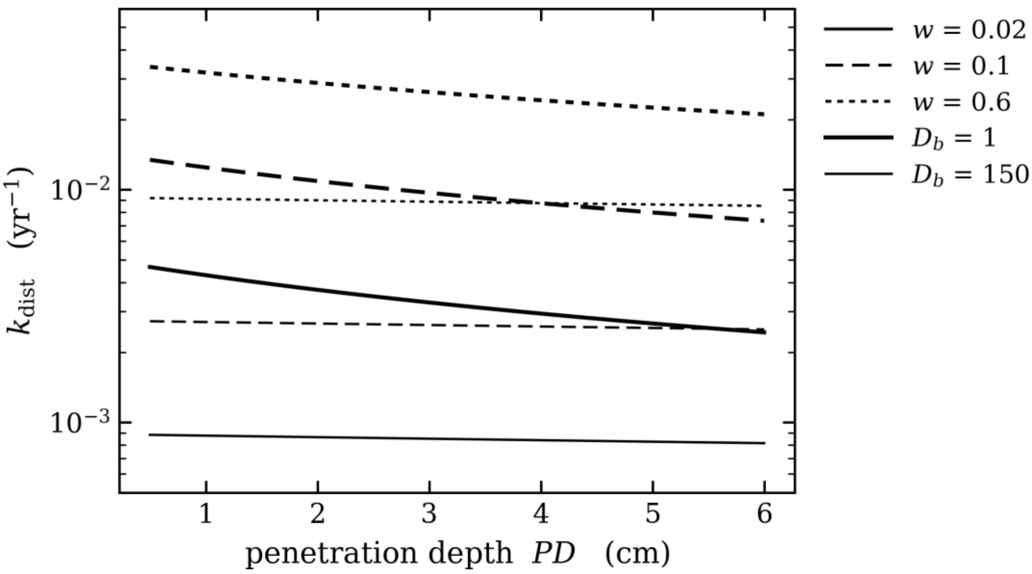

Figure S3. *How k_{dist} changes as the gear cuts deeper. Three accumulation rates are shown, given in the key in cm yr^{-1}, and two mixing intensities. Thick lines are weak mixing, D_b = 1 cm^2 yr^{-1}, and thin lines are strong mixing, D_b = 150 cm^2 yr^{-1}.*

Cutting deeper always lowers the rate constant, because deeper material is older. The effect stops growing once the gear passes the depth that mixing has already stirred smooth. Where mixing is strong the curves are nearly flat, and that is why the cutting depth explains so little of the spread.

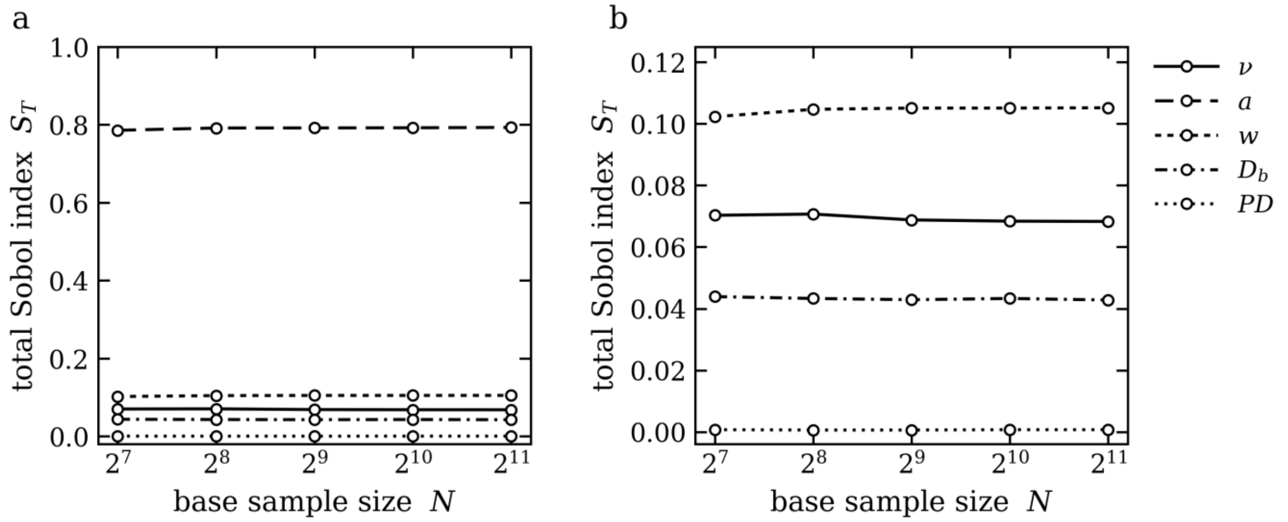

Figure S4. *The five shares of the spread, plotted against the size of the sample used to compute them, from 128 to 2048. A converged value is one that stops moving as the sample grows. (a) The full scale. (b) The same data on an axis that fits the four small shares, which cannot be told apart in panel (a).*

The ranking is already final at the smallest sample plotted, 128. Between 512 and 2048 no index moves by more than 0.0013, so the values quoted in the main text are converged.

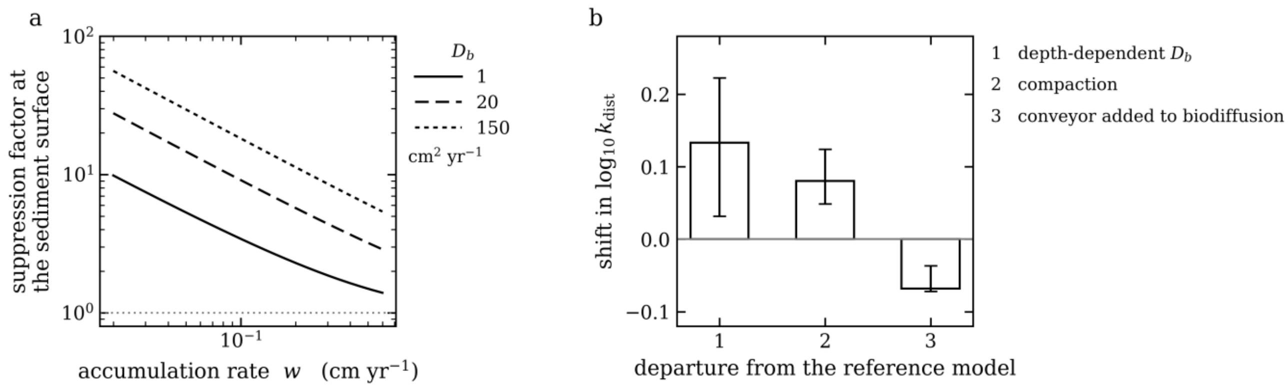

Figure S5. *(a) How much less reactive the sediment surface is than the material landing on it, plotted against the accumulation rate for three mixing intensities. The grey dotted line marks a factor of one, which is where there would be no loss at all. (b) How far three of the departures in Table 5 of the main text move $\log_{10} k_{dist}$. The departures are named in the key at the right. The depth-dependent case shown is the deep mixed layer, z_0 = 10 cm. Bars are medians, and the whiskers cover every case tested.*

None of the three moves the answer by as much as a quarter of a decade. Together they span −0.09 to +0.22. The third has the opposite sign to the first two, so they partly cancel instead of adding up.

Two other departures are deliberately left off this axis. The seasonal result is a swing between a high and a low, not a shift in one direction, so it does not belong on the same scale. Replacing mixing by a conveyor is about ten times larger than anything drawn here and would flatten the rest. Each has its own figure, S7 and S6.

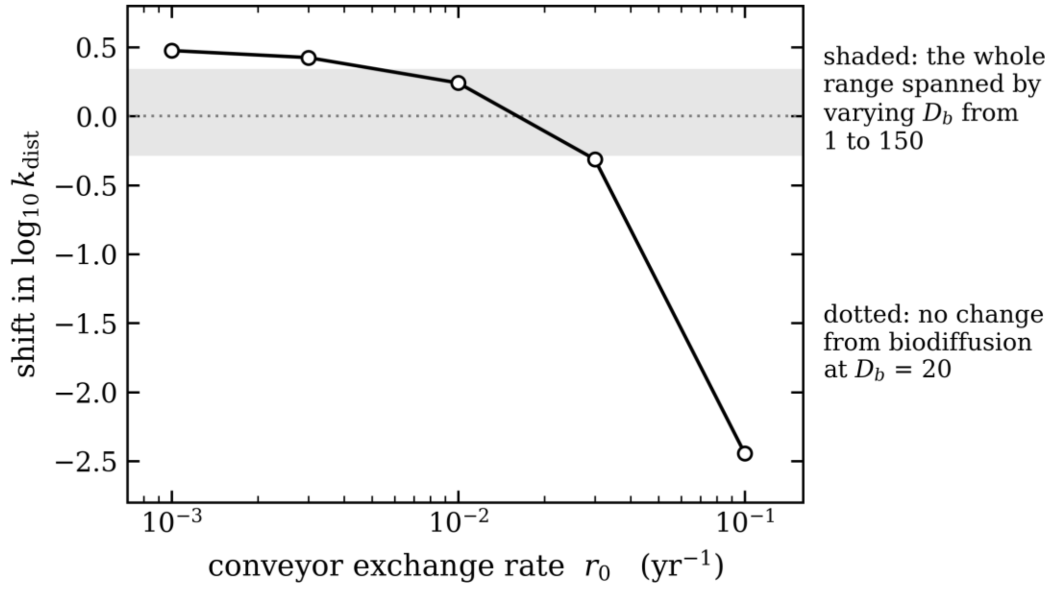

Figure S6. *What happens when stirring by animals is replaced by a conveyor, meaning animals that feed at depth and drop the material back at the sediment surface. The vertical axis is the resulting shift in $\log_{10} k_{dist}$, and the horizontal axis is how fast the conveyor turns the bed over. The shaded band is the whole range covered by varying D_b from 1 to 150 $cm^2\ yr^{-1}$ with ordinary stirring, so a curve that leaves the band has moved further than the coefficient ever could.*

The curve leaves the band, and it crosses zero at a turnover rate of 0.019 yr^{-1}. How the mixing is represented therefore matters more than how strong it is. The Sobol index of D_b cannot show this, because that index only varies a number inside one way of representing mixing, not the representation itself.

The sweep stops at 0.1 yr^{-1}. Two faster rates were computed, but at those rates a perfect conveyor is no longer a believable picture of a real bed, and drawing them would set the axis by numbers the main text does not defend.

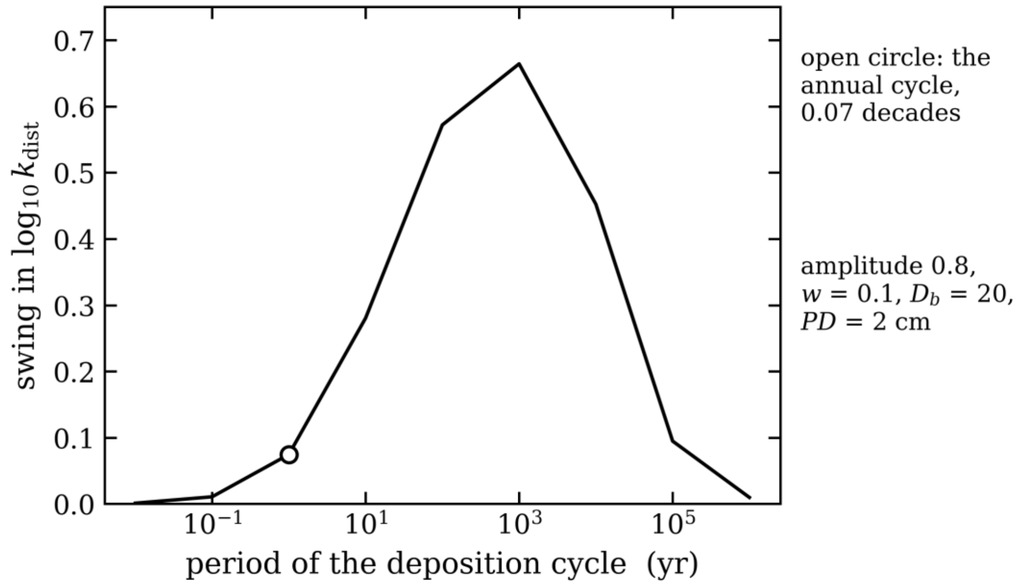

Figure S7. *How far k_{dist} swings over one cycle when the supply of carbon to the seabed rises and falls, plotted against how long that cycle lasts. The amplitude of the supply cycle is 0.8, at $w = 0.1$ $cm\ yr^{-1}$, $D_b = 20\ cm^2\ yr^{-1}$ and $PD = 2$ cm. The open circle marks a cycle of one year.*

The swing falls to zero at both ends. Fast cycles are smoothed out by the bed before they reach the disturbed layer. Very slow cycles are close to steady, and a ratio does not change under a steady change in supply. The swing is largest for cycles of about a thousand years. The annual cycle, which is the one a shelf bed actually sees, sits on the low side of that peak at 0.07 decades.

S2 Reference implementation

The whole model is three short routines, printed below. The first builds the mixture of reactivities. The second solves for how each part of that mixture falls off with depth. The third averages over the layer the gear reaches. The code that runs is identical to the deposited file T1_core.py, line for line. Only the comments differ, and they were shortened to fit the page. Everything else, meaning the checks, the sweeps, the Sobol indices and the seven sensitivity analyses, is in the other fifteen deposited scripts.

```
KMIN, KMAX, NK = 1e-14, 1e4, 20000          # stated in Table 4

def classes(nu, a, n=NK, kmin=KMIN, kmax=KMAX):
    """Reactivity grid, the deposited mass density on it, and the inert mass
    below kmin. No normalisation is applied: the gamma density already
    integrates to one over (0, inf), and the mass below kmin is returned
    separately rather than redistributed."""
    k = np.logspace(np.log10(kmin), np.log10(kmax), n)
    g = a**nu * k**(nu-1) * np.exp(-a*k) / GAMMA(nu)
    m_inert = gammainc(nu, a*kmin)          # regularised lower incomplete gamma
    return k, g, m_inert


def lam_of(k, w, Db):
    """The decaying root of Db lam^2 - w lam - k = 0, written so that it
    does not cancel catastrophically when 4 Db k is much less than w^2."""
    return -2.0*k / (w + np.sqrt(w*w + 4.0*Db*k))


def profile(k, g, m_inert, w, Db, PD):
    """Mass-weighted rate constant of everything above depth PD,
    Eqs. (3) to (6)."""
    lam  = lam_of(k, w, Db)
    C0   = g / (w - Db*lam)                 # flux condition, Eq. (4)
    I    = C0 * np.expm1(lam*PD)/lam        # depth integral, Eq. (6)
    mass = np.trapezoid(I, k) + m_inert*PD/w  # the k -> 0 component carries mass only
    rate = np.trapezoid(k*I, k)
    return rate/mass                        # Eq. (5)
```